REPORT NO.
63270-00-02
MAY 1961

SECOND QUARTER[illegible]OGRESS REPORT

LIQUID PROPELLANT LOSSES DURING SPACE FLIGHT

PREPARED FOR
THE NATIONAL AERONAUTICS
AND SPACE ADMINISTRATION
CONTRACT NO. NAS5-664

LIQUID PROPELLANT LOSSES DURING SPACE FLIGHT

SECOND QUARTERLY PROGRESS REPORT

MAY 1961

Report No. 63270-00-02

Arthur D. Little, Inc.
Cambridge, Massachusetts

Approved for distribution by:

Norman M. Wiederhorn
Project Director

Prepared

for

NATIONAL AERONAUTICS AND SPACE ADMINISTRATION
OFFICE OF LAUNCH VEHICLE PROGRAMS
LIQUID ROCKET ENGINES PROGRAM

Contract Number NAS5-664

ACKNOWLEDGMENTS

The following personnel of Arthur D. Little, Inc. were associated with this program:

Igor A. Black	David A. Knapton
Russell J. Bowen	David B. Lull
S. Edward Eaton	D. Read Moffett
John R. Ehrenfeld	James L. Schad
Alfred G. Emslie	Peter F. Strong
Robert P. Epple	Robert O. Teeg
Peter F. Glaser	Virginia R. Valeri
El Ahmadi I. Heiba	Norman M. Wiederhorn
Ann J. Jordan	

We should also like to acknowledge the assistance of the following university personnel who worked as consultants for us on this program:

Professor Robley D. Evans, Department of Physics, Massachusetts Institute of Technology

Professor Sydney Goldstein, Chairman, Department of Applied Mathematics, Harvard University

Professor Gerald V. Bull, Department of Engineering Sciences, McGill University

We should also like to acknowledge the assistance of Mr. Oscar Bessio of NASA Headquarters and Dr. R. J. Brun of the NASA Lewis Research Center in the conduct of this work.

TABLE OF CONTENTS

LIST OF FIGURES

LIST OF TABLES

I. INTRODUCTION

A. PROGRAM OBJECTIVES

As described in our first quarterly progress report, the basic objective of this program is to provide evaluation techniques, methodology and data which will permit the design engineer to evaluate liquid propellant storage system concepts and to design optimum systems for vehicles for any mission within the solar system. In order to achieve our objectives our approach is to describe quantitatively those aspects of the environment which may be contributory to propellant losses, the interactions of the propellant and its storage system with the environment and finally the performance of protective systems to limit such losses. The program has been divided into four principal areas for study. These are:

1. The space environment.
2. The interaction of thermal radiation with the propellant and its storage system.
3. The interaction of meteoroids with the propellant and its storage system.
4. The interaction of ionizing radiation with the propellant and its storage system.

B. SUMMARY OF WORK PERFORMED DURING THE SECOND QUARTER

Work on the major aspects of this program may be summarized as follows:

1. A Space Environment

We are continuing to gather the published information on the space environment and to interpret its significance. By and large the major effort here was completed during the first quarter of the program and is included in the first quarterly report. We do not intend to update this report in each quarter but rather will report on the more significant events which have occurred during the previous quarter.

During this past quarter we have continued to accumulate information and have initiated a punch-card system for filing and retrieving the information.

2. Study of Thermal Interactions

Our study of the thermal interactions of the space environment with liquid propellants and their storage systems is proceeding along three lines, namely, theoretical studies, analytic studies of thermal protection systems, and experimental studies of insulations. In the theoretical studies we have studied the influence of spacing of multilayer thermal radiation shields on the performance of such shields and have shown that even in ideal shields at very low temperatures the performance can be expected to be a function of the spacing between shields (Report No. 63270-04-02 by A. G. Emslie). We have also conducted a theoretical study of the influence of gas pressure within multiple-layer radiation shields upon their performance (Report No. 63270-04-01 by A. G. Emslie). This study includes a discussion of the effects of outgassing from shields upon their performance.

Our analytic studies have been pointed at the development of a computer-based program for designing optimum thermal radiation shielding systems for cryogenic propellant storage tanks. As a consequence of the work conducted during this past period, we have succeeded in developing a generalized mathematical formalism to achieve this objective. The factors which are taken into consideration include:

1. various radiative heat inputs, i.e., direct solar radiation, planet shine and radiative inputs from other portions of the vehicle.
2. heat leaks to the propellant tank from struts, pipes and other structural members.
3. mission requirements for any flight within the solar system.

A report describing this work is now being prepared. It will be issued as Report No. 63270-04-03 by J. Ehrenfeld and P. Strong.

Our major effort relating to the experimental program concerned with the thermal interactions has been devoted to the design and construction of an apparatus for measuring the performance of insulations at temperatures to 4°K. This equipment has been designed and is now under construction. With the equipment we will be able to measure the thermal conductivity of insulating materials as a function of insulation thickness (number of shields in multiple-layer radiation shielding), temperature difference, gas pressure and mechanical loading. The equipment will also be useful for determining the effects of heat leakage through struts and joints in multiple-layer radiation shielding.

3. Study of Meteoroid Interactions

The work on this aspect of the program has been concerned primarily with the evaluation of "meteor bumpers" as protective devices against the meteorite hazard. In addition we have given consideration to other protective schemes which might be employed.

The study of meteorite bumpers has been both theoretical and experimental. A first order theory has been developed to attempt to explain the performance of meteor bumpers. This theory is based upon a simple mechanical model. However, the experimental results which we have gathered to date indicate that this theory may be over-optimistic with respect to estimating the protection that bumpers will afford. In view of this we have undertaken a more detailed theoretical study of the physics of the break-up of particles when they penetrate thin metal targets. The basic approach in this study is concerned with a consideration of the shocks which travel through both the bumper material and the projectile after impact, and how these in turn cause the break-up of the particles. This work, which is still preliminary in nature, indicates that the break-up is highly dependent upon the particle shape, the attitude with which a non-spherical particle strikes the bumper, the density of both the bumper material and the projectile, and the equation of state of these materials. In spite of the very preliminary nature of this work, the concepts developed in the study have been useful in formulating a qualitative explanation for some of the experimental results which we have obtained.

In addition we have given consideration to the development of a protection system in which meteoroids are detected while they are distant from the vehicle and then either a bumper is positioned in the meteoroid path, or the vehicle is moved out of the path of the particle. In particular we have concerned ourselves with estimating the available time for executing a protective maneuver if the meteoroids are observed by optical means. For particles in the size range of interest, i.e., 0.01" to 1" diameter, the available maneuvering time is between 10^{-1} to 10^{-4} seconds. If a ten-foot motion of either a shield or the vehicle is required for protective purposes, an acceleration of 10^{2} to 10^{8} g will be necessary. The large power requirements to achieve even the minimum acceleration for any reasonable size shield or vehicle, would appear to preclude this as a practical approach to the solution of the meteoroid problem.

As a consequence of this work, we are of the opinion that optical sighting may be a useful method for obtaining meteoroid data in satellite experiments. The area enclosing the volume of space which can be observed by optical methods is much larger than the area which is observed by the instrumentation which is currently used aboard satellites. We have not attempted to design a detector based upon optical methods.

4. Study of Ionizing Radiation Interactions

During this period of the work a more detailed analysis has been made of the radiation dosage resulting from high energy protons and from bremsstrahlung accompanying the absorption of electrons in the outer Van Allen belt. This study has been carried out by the use of parametric methods which can be applied to any spectrum of incident radiation. The results are presented in a form such that it is possible to calculate the dosage within a volume at any distance from the surface of the vehicle. The procedures which have been developed have the advantage of flexibility and avoid the errors that result from other procedures which assume a previously determined distribution function for the

radiative energy. The results are applicable both for the storage of propellants as well as for calculating the dosages which will be received by any object, living or inanimate, behind a barrier.

In addition a more detailed analysis has been made of the possible magnitude of radiation effects on the mechanical properties of several structural materials. The possibility of hydrogen embrittlement of stainless steel resulting from diffusion of either molecular or atomic hydrogen has been estimated to be negligible. The possible effects of radiation on the emissivity of surfaces has also been estimated in the case of aluminum metal covered by electrolytically deposited oxide layers.

5. Other Activities

During this past period we have briefed several NASA contractors on our work to date and our planned program. We have also provided them with technical assistance on a consulting basis. These include personnel from General Electric, Avco, and Pratt and Whitney. We have found such meetings with other contractors mutually profitable as interchange of ideas and background material has been quite free and open.

We have also undertaken a review of the Zero G studies which have been conducted to date. Our effort here has been solely concerned with studies concerning liquids in vessels. Although our work in this area has been preliminary, we have been able to demonstrate that in a Zero G environment and at thermodynamic equilibrium, a liquid in a closed vessel will partially wet the wall unless the contact angle is precisely 0° or precisely 180°. This is at variance with the previously published concepts that the liquid will be either on the wall or as a large mass in the tank with the vapor on the wall.

II. THERMAL INTERACTION STUDIES

A. INTRODUCTION

During the past quarter, our activities have consisted of the continuation of our efforts to isolate and define important problem areas raised by the thermal environment and the initiation of a number of studies with the objective of providing a general and accurate procedure for the analysis and design of thermal protection systems.

Our literature survey of publications in the area of thermal problems and system analysis has continued and seems to be reasonably complete and up to date.

The first two studies outlined below were specific efforts to investigate certain theoretical aspects of the behavior of multiple-foil radiation shielding. Individual reports describing the details of these studies have been distributed (Report Nos. 63270-04-01 and 63270-04-02). The remaining items are points drawn from a larger study to develop methods for design and performance analyses. A technical report on work to date is in its final stages of writing and will be published during the next quarter.

B. THEORETICAL ASPECTS RE THE BEHAVIOR OF MULTIPLE-FOIL RADIATION SHIELDING

1. Gas Conduction Problems

On a long mission in space, a cryogenic fuel tank may require radiation shielding consisting of as many as 100 sheets of low-emissivity metal foil, if heat is transferred through the shielding only by radiation. If gas conduction also occurs, more foils will be needed to maintain the same rate of fuel boil-off.

The effect of gas pressure on conduction can be expressed in terms of the ratio of foils required with gas conduction to the theoretical number for radiative transfer alone.

$$\frac{n}{n_o} = 1 + ap \qquad (1)$$

where p = gas pressure in mm Hg

n = number of foils with gas conduction

n_o = number of foils as $p \longrightarrow o$

and a is a constant which depends upon the temperatures of the outermost and inntermost foils, the gas which is between the foils, and the emissivity of the foil material.

The constant "a" may be given as

$$a = \left(\frac{2}{\epsilon} - 1 \right) \left(\frac{9RT_1}{2\pi M} \right)^{1/2} \left[(T_2/T_1)^{1/2} - 1 \right] \Big/ \sigma(T_2^4 - T_1^4) \qquad (2)$$

where ϵ is the emissivity of the shield

T_1 and T_2 are the temperatures of the coldest and hottest shields, respectively

R is the gas constant

and M is the molecular weight of the gas in the volume between the shields.

Values for the constant "a" for various gases at various values of T_1 are given in Table I. In calculating this table, it was assumed that ϵ is 0.05 and T_2 is 300°K. The units of "a" are $(\text{mm Hg})^{-1}$.

TABLE I

VALUES FOR THE CONSTANT "a" IN EQUATION 1
FOR VARIOUS GASES AND INTERNAL TEMPERATURES

T_1 in °K	"a" x 10^{-3}				
	Helium	Hydrogen	Oxygen	Nitrogen	Neon
20	6.1	8.7			2.8
77	4.1	5.8	1.5	1.6	1.8
90	3.7	.3	1.3	1.4	1.7

Using the values for "a" of Table I in equation 1, it is seen that if n/n_o is to be maintained below a value of 2 if liquid hydrogen is stored and hydrogen is the gas in the volume between shields, then the gas pressure in the shields should be less than about 10^{-4} mm of Hg. For the storage of liquid O_2, the pressure should be less than about 5×10^{-4} mm Hg. In view of this, if outgassing of the shields or gas diffusion from the fuel tank are appreciable, it will be difficult to design and construct an adequate sealed-off, evacuated shield.

It is also difficult to arrange the geometry of the shields to use the external space vacuum for pumping. In the case of pumping through the edges of a 100-cm wide shield panel, the outgassing rate should not exceed about 10^9 molecules sec^{-1} from each cm^2 of shield surface, in order to prevent an inordinate increase in the number of shields which are requied. The maximum allowable outgassing rate for broadside pumping of optimally perforated foils is of the order of 10^{10} molecules sec^{-1} cm^{-2} of shield surface. In this latter situation, a basic consideration is that any geometrical arrangement of perforations in the foils that enhances pumping of the gas, also reduces the effectiveness of the foils as a radiation shield, since radiation can enter by the same path by which molecules leave.

The effect of perforations can be expressed in terms of an effective emissivity, ϵ^1

$$\epsilon^1 = \epsilon + (2-\epsilon)\tau$$

where ϵ^1 is the effective emissivity

ϵ is the true emissivity of the foil

and τ is the fraction of the foil area which is holes.

If there is a given constant outgassing rate from the foils, then there will be an optimum value for τ, for a given number of foils in the multifoil radiation shielding. This value can be obtained from the relation

$$\frac{\tau}{1-\tau} = \left[\frac{3}{4}\nu\, k(T_2-T_1)(2-\epsilon)n \Big/ \sigma(T_2^4 - T_1^4)\right]^{1/2} \qquad (4)$$

where ν is the rate of outgassing in molecules per cm^2 per sec., k is the Boltzmann constant and n is the number of shields.

The corresponding minimum value of the heat flux through the shields is

$$q_{min} = \frac{\sigma(T_2^4-T_1^4)}{(\frac{2}{\epsilon} - 1)n} + \left[\frac{6\nu k}{n}(T_2-T_1)\sigma(T_2^4-T_1^4)(\frac{2}{2-\epsilon})\right]^{1/2} + \frac{3}{2}\nu k(T_2-T_1) \qquad (5)$$

If q_o is the heat flux for an absolute vacuum between the shields and no outgassing (thus $\tau = o$), the ratio of q_{min} to q_o for various outgassing rates is given in Table II. This Table was calculated for $T_2 = 300°K$, $T_1 = 25°K$, $\epsilon = 0.05$ and $n = 100$.

TABLE II

RATIO OF MINIMUM HEAT FLUX WHEN SHIELDS ARE OUTGASSING TO THAT FOR PERFECT VACUUM BETWEEN SHIELDS

ν (molecules/cm^2/sec)	q_{min}/q_o
10^{11}	1.1
10^{12}	1.3
10^{13}	1.9
10^{14}	3.8
10^{15}	10.2

It is apparent from Table II that for effective multi-foil radiation shield performance outgassing rates must be small.

2. Radiation Transfer by Closely-Spaced Shields

The usual formula for radiation transfer through a stack of radiation shields breaks down when the spacing of the shields is less than the wavelength of the peak of the black body spectral distribution corresponding to the temperature of the shields. Two effects set in

at these close spacings -- wave interference and radiation tunneling. Wave interference of the emitted radiation occurs in the narrow gaps between the shields and may increase or decrease the energy transfer, depending on the spacing. Radiation tunneling allows transfer of radiation that ordinarily suffers total internal reflection inside the shield material. This effect gives an energy transfer that increases exponentially as the spacing decreases. The two effects together give an energy transfer rate per unit area which becomes, in the limit of zero spacing,

$$q = \frac{n^4}{n^2 + k^2} \sigma (T_2^4 - T_1^4) \qquad (6)$$

where n and k are the real and imaginary parts of the complex refractive index, σ is the Stefan-Boltzmann constant, and T_2 and T_1 are the temperatures on the two sides of a gap.

The formula implies that the radiation density e' and velocity of propagation c' in the shield material are

$$e' = \frac{n^2 \sigma T^4}{c}$$

$$c' = \frac{n^2 c}{n^2 + k^2}$$

For moderate values of the absorption index k, the flux formula predicts a transfer rate between two close shields greater than that between two black surfaces.

In the case of metal shields, when the spacing between the two shields is increased from zero, the radiation transfer rate at first rises sharply to a high maximum and then falls below the usual value for widely-spaced shields. The flux returns to the normal level when the spacing exceeds about one-half of the wavelength of the black body peak. Figure 1 shows the transfer rate as a function of spacing for a material in which n = 1.5, and k = 10. In this figure the abscissa is the ratio of

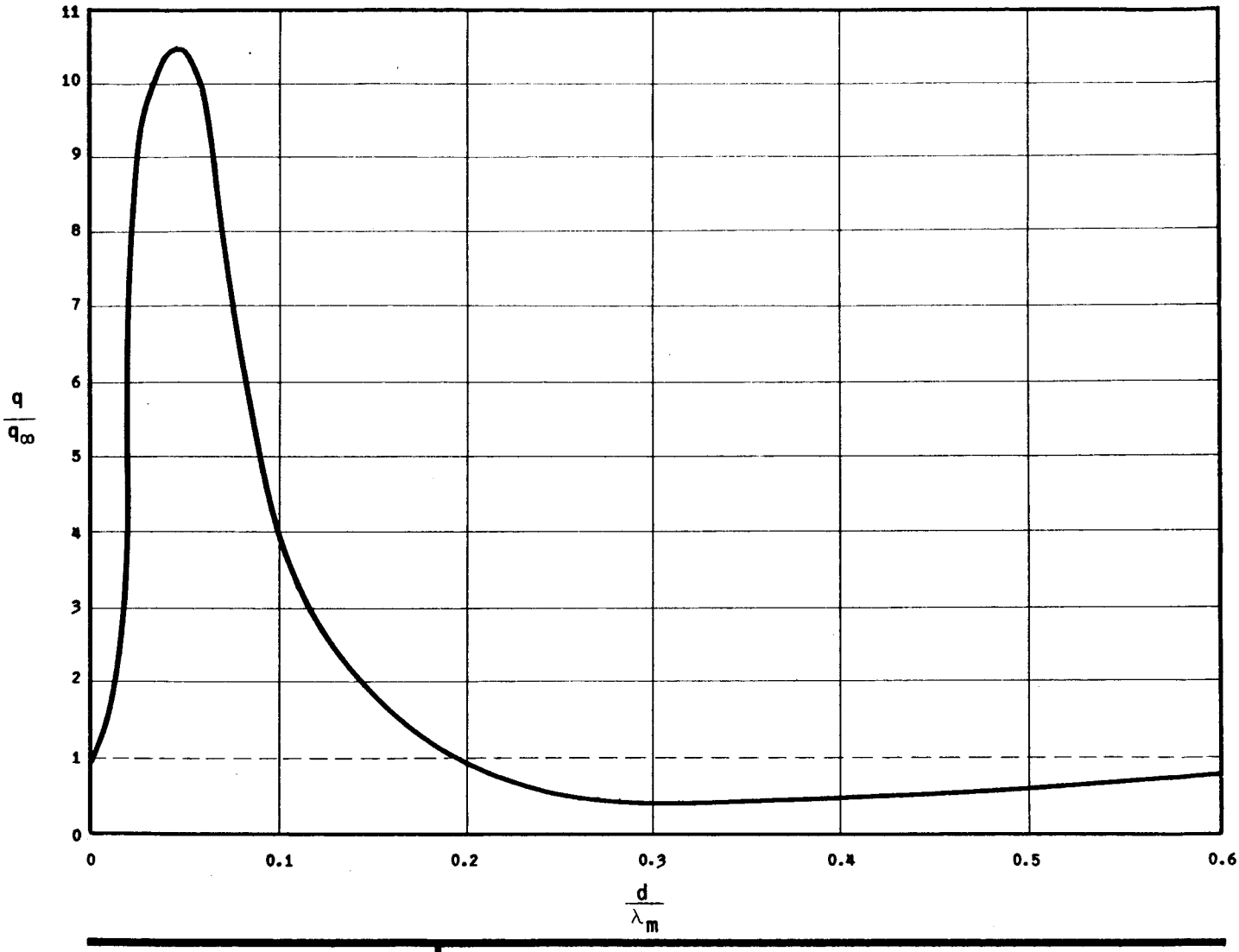

FIGURE 1 | Heat Transfer Rate as Function of Spacing

foil spacing to the peak wavelength of the black body curve and the ordinate is the ratio of the radiation flux at this spacing to the flux which would be observed at infinite spacing.

Figure 1 does not include the transfer of radiation which tunnels through the foil-gap interface. It only shows the flux which would result if there were no tunneling. We have not arrived at a quantitative expression for the tunneling phenomenon as yet. However, the effect of tunneling through the interface is to increase the overall radiation flux at small spacings between foils. Thus, this will contribute an additional flux to that shown in Figure 1.

It is interesting to note the spacing between foils at which these phenomena will begin to be of concern. The wavelength of the peak of the black body emission curve is given by

$$\lambda_m = 2897/T \tag{7}$$

where λ_m is given in microns and T is in degrees Kelvin.

This effect commences when the spacing between shields is approximately $0.5\lambda_m$ (see Figure 1), or

$$d_c = 1449/T \tag{8}$$

where d_c is the shield spacing in microns where this effect commences. In the case of the storage of liquid oxygen (T of inner shield $\cong$ 90°K) spacings which are less than approximately 16 microns (0.6 mils) should be of concern. For the storage of liquid hydrogen this becomes 58 microns (2 mils) and for liquid helium 350 microns (14 mils).

C. ANALYTIC STUDIES OF THERMAL PROTECTION SYSTEMS

The design of a thermal protection system for cryogenic fluids aboard a space vehicle is intimately associated with the overall vehicle design and the mission for the vehicle. Previous work (1-3) has indicated that it should be possible to store cryogenic liquids for extended periods of time in space. Our calculations have confirmed this con-

clusion. Thus, it appears that it will be possible to carry materials such as liquid hydrogen or liquid helium on trips to Mars and Venus and return.

Unfortunately, the work which has been reported earlier has considered idealized systems. The models chosen for the vehicle and the liquid storage tank did not consider structural members for the purpose of supporting the tank with its insulation, pipes to connect the insulated tank with a motor or other portions of the vehicle or seams and joints which will be present in the insulation as a result of fabricating the tank. All these factors will lead to heat leaks to the cryogenic liquid. Furthermore, in these analyses in all cases it was assumed that the insulating material would be multilayer radiation shielding. Although this is very reasonable, the calculations were performed assuming idealized shielding with no heat leaks through spacers or other components of the shielding.

1. Performance Criterion For Thermal Protection Systems

Although this earlier work was of considerable value, it offers little assistance to the engineer who is concerned with the design and construction of a storage system for a particular vehicle which has a specific mission to perform. The objective of the work that we have undertaken is to provide a more detailed background and procedures to assist the designer in planning and constructing a vehicle. We hope to set useful criteria and procedures for him and indicate approaches which he may profitably employ. The basic criterion in our work, which is the same as that used by other workers, is that there is a payload penalty associated with the storage of cryogenic propellants in space. This penalty is made up of two components, namely, the weight of insulation which is carried aboard the vehicle and the weight of propellant which is lost during the journey due to boiloff. It is apparent that any storage system design should have as its major objective the minimization of this penalty, consistent with other factors which influence the design of the vehicle.

The payload penalty is given simply as:

$$W_{PEN} = W_{TPS} + \lambda W_{LOSS} \tag{9}$$

where W_{PEN} is the payload penalty, W_{TPS} is the weight of the thermal protection system, W_{LOSS} is the weight of propellant jettisoned during the voyage and λ is a constant which takes into consideration the fact that the propellant which has been jettisoned during flight need not be decelerated when the engines are turned on. λ is dependent upon the mission requirements as well as the design of the vehicle, and is given as:

$$\lambda = 1 + \frac{K_T}{\rho^o}(1+u) - (1-R)(1+K_o)\left[1+(1+u)\frac{K_T}{\rho o} + \frac{K_M}{1+K_o}\right] \tag{10}$$

where

K_T = ratio of tank weight to propellant volume

ρ^o = propellant density

u = ullage fraction

K_o = outage fraction

K_M = miscellaneous fraction

$R = \exp\left\{-\Delta v/I_s g\right\}$

Δv = incremental velocity requirement

I_s = propellant specific impulse

g = gravitational constant

The use of such a simple index as a criterion for establishing a design of a vehicle belies the complexity of determining the quantities of which it is constituted. Techniques for the determination of the boil-off loss terms are discussed below.

2. General Discussion of Boiloff Losses

The amount of propellant jettisoned during a space voyage in a regulated-pressure storage system is

$$W_L = \frac{1}{L_E} \int_{t_B}^{t_F} \dot{Q}_T dt \qquad (11)$$

The time, t_B, when boiling commences depends on the initial state of the system and on the pressure-regulator set-point. For systems, where the propellant is loaded as a solid or as a subcooled liquid, the time, t_B, is determined from the following equation.

$$\int_{t=o}^{t_B} Q_T dt = \overline{\Delta H} \qquad (12)$$

where

$$\Delta H = W_p^o \left[C_S(T_M - T_o) + L_M + C_L (T_B - T_M) \right] \quad \text{for } T_o < T_M \qquad (13a)$$

$$= W_p^o \; C_L(T_B - T_o) \quad \text{for } T_o > T_M \qquad (13b)$$

and

L_E = latent heat of evaporation

$\dot{Q}_T$ = total heat leak rate to tank

t = time

t_F = light off time

W_p^o = initial propellant weight

C_S = heat capacity of solid propellant

C_L = heat capacity of liquid propellant

T_M = melting point

T_B = boiling point

T_o = initial propellant temperature

L_M = latent heat of fusion

It is convenient to combine the above equations and eliminate the need for calculating t_B.

$$W_L = \frac{1}{L_E} \int_{t=o}^{t_F} \dot{Q}_T dt - \frac{\Delta H}{L_E} \qquad (14)$$

Except for the subtractive term depending on initial conditions, the magnitude of weight loss depends on the behavior of heat flow to the tank, $\dot{Q}_T$, as a function of time.

The most desirable approach toward a general description of $\dot{Q}_T$ would be the development and solution of a rigorous and analytic model for the flow of heat in a complex system including a propellant storage tank, a thermal protective system, and structural appendages of the tank. Although the heat transfer equations have been studied extensively and solutions exist for many real physical situations, certain aspects of propellant storage systems preclude their direct application in this situation. This is due to the following characteristics of the system.

1. It seems certain that multiple-foil radiation shielding will be the basic insulation in the thermal protection systems of presently programmed and next-generation space vehicles using cryogenic fluids. Such materials differ from most insulating media in that the heat con-

ductivity through them is neither linear nor isotropic. Also, the materials are inhomogeneous. The primary mechanism of heat transfer is by radiation and not conduction. This leads to the non-linear behavior. In addition, the conductivity perpendicular to the surface of the insulation is very much less than in the plane parallel to the surface, leading to anisotropy. Also although in theoretical considerations it is usually assumed that heat transfer is solely by radiation, measured values for the thermal conductivity of representative materials indicate that appreciable conduction exists (4-7).

2. A complete storage system is naturally complex, with at least three major components, the tank, a thermal protection system, and structure to unite the tankage to the operational portions of the vehicle. A separate equation must be written for each portion of the system defined by boundaries where two or more materials are joined or where the geometry changes. The prime difficulty that this introduces is the need to specify the conditions at each boundary. In most cases, precise boundary conditions cannot be written.

3. The primary boundary conditions expressing the interaction with radiative inputs and the surface of the storage system are non-linear and time-varying. Analytic methods have not been developed for such cases, except for a few very simple physical situations (8).

In order to utilize the rigorous phenomological equations for heat transfer in the face of the obstacles raised by the above characteristics, several approximations can be made which permit the rigorous form to be maintained. These are:

1. Heat inputs through the primary insulation and through structural appendages are independent.

2. Multiple-foil radiation shielding can be treated as a homogeneous but anisotropic conductor in which the conductivity normal to the surface is a function of the boundary temperatures. This permits the use of measured values of effective mean thermal conductivity.

3. The insulation can be divided into zones of simple geometry.

4. The resistance to heat flow in the tank wall relative to the resistance in the shielding is so low that no gradient exists in the tank wall. This is equivalent to assuming that the inner wall temperature of the insulating skin is at the propellant temperature.

5. The system is in quasi-static equilibrium with the instantaneous input energy flux, i.e., the temperature distribution is governed by a solution of Laplace's equation with time-varying boundary conditions.

(The justification for these approximations are presented in part in the next paragraphs. They will be presented in detail in the technical report devoted to this subject.)

According to the first assumption, the total heat leak to the tank can be written

$$\dot{Q}_T = \dot{Q}_R + \dot{Q}_C \tag{15}$$

where $\dot{Q}_R$ is the heat leak through the insulation and $\dot{Q}_C$ is the heat leak through the structures. The two factors on the right are assumed independent. The approach toward a general technique for evaluating each of these factors will be different. The heat leak through the insulation is the simpler of the two since the choice of a particular structural design does not affect the mechanism of heat transfer, but

only the magnitude of the losses. Thus, in seeking general insulating design criteria only a small number of geometries and situations need be considered. Also, the use of an effective mean thermal conductivity as the primary parameter of insulation media (approximation 2 above) permits a general statement for performance to be written, using standard techniques, in spite of the conduction mechanism of the insulation. Thus, the analysis will be valid for any insulation, including multiple foil, evacuated powder and conventional.

On the other hand, the heat leak through structural members is very dependent on the design of the overall vehicle. Since the design of such structures probably will be dictated by considerations other than to provide a minimum heat leak, the development of a general model for the heat leak through structures will be much more difficult than through the insulation.

Anticipating the results of our study so far, this appears to be the case. The results of the study on heat leak through insulation appear to be sufficiently complete and general to permit consideration of a computer program which requires only a few input parameters. On the other hand, the work on the heat leak in structural members has progressed only to the point where the rough form of a technique is suggested. However, even at this stage it is apparent that a larger number of parameters will be required to specify the structural aspects.

3. Approximate Methods

On the basis of approximation number 3 above, it is possible to consider the tank as a number of separate sections of simple geometry, i.e., plane, cylindrical and spherical surfaces. The procedure then is to calculate and optimize the insulation for each section. It should be pointed out that this model need not limit the precision of the calculation of the heat leak. The error associated with this approximation can be decreased to any desired value by subdividing the tank surface into more surfaces for consideration.

The next question which arises in this model is the method for treating the interactions between adjacent sections or areas of the tank. As noted previously, multiple-foil radiation shielding is anisotropic in that heat conduction perpendicular to the surface is markedly less than parallel to the surface. There are two extreme conditions which may be considered. In one, the conduction parallel to the surface is infinite and as a result the skin assumes a uniform temperature. This assumption is implicit in the treatment given by Smolak and Knoll (2,3) and Burry and Degner (1). The other extreme is to consider the conduction parallel to the surface to be appreciable compared to the conduction perpendicular to the surface, but nevertheless a small absolute value. This is equivalent to stating that each section of the surface comes to an equilibrium temperature which is determined by the heat flux to that section of the surface and is not influenced by the adjacent sections. This case is a conservative one in that the calculated heat leak to the liquid is greater than would be experienced in practice. The assumption of a uniform skin temperature (infinite surface conduction) predicts smaller heat leaks than will actually occur. We have chosen the conservative assumption for initial consideration. We have unsuccessfully attempted to find general algebraic solutions for the intermediate case where the surface conductivity is appreciable, but finite. Instead we are trying to develop simple numerical solution techniques.

By considering small areas on the surface over which the radiant input is reasonably uniform, the heat leak can be calculated by algebraic techniques as follows:

In any one section of the surface the balance between input radiation and the sum of reradiated and transmitted heat flux is

$$I = \eta\epsilon_o \sigma T_s^4 + \frac{\beta k}{\delta}\left[T_s - T_p\right] \qquad (16)$$

where

I = total input per unit area to the section

ϵ_o = emissivity of surface

σ = Stephan-Boltzmann constant

T_s = surface temperature

T_p = propellant temperature

k = radial conductivity of insulation

δ = insulation thickness

η, β = geometrical factors

Once the input is specified, this equation can be solved for T_s, which is subsequently required to determine the heat leak to the propellant.

In general this technique involves the solution of a quartic equation. For the specific case of a well-insulated tank, i.e., where the reradiation term is large compared to the transmitted term, i.e.,

$$\eta e_o \sigma T_s^4 >> \frac{\beta k}{\delta} \left[T_s - T_p \right] \tag{17}$$

the solution can be approximated by assuming that the skin temperature differs from that of a perfect insulator by a linear perturbation. The result of this is

$$T_s = T^o \left[1 - \frac{\beta k}{4\delta I} (T^o - T_p) \right] \tag{18}$$

where T^o is the solution corresponding to the perfect insulator and is given by

$$T^o = \left[\frac{I}{\eta e_o \sigma} \right]^{1/4} \tag{19}$$

The total heat leak to the tank is obtained by summing the contributions for each section, i.e.

$$\dot{Q}_c = \Sigma \frac{\beta_j k_j A_j}{\delta_j} \left[T_{s_j} - T_p \right] \qquad (20)$$

where A_j = area of jth section.

This expression can be treated analytically in determining the optimum insulation thickness for each section.

4. Optimum Insulation Requirements

The criterion for an optimum insulating system is that the payload penalty should be a minimum. As noted previously, this is given as

$$W_{PEN} = W_{ins} + \lambda W_{LOSS} \qquad (9)$$

Having fixed the tank dimensions, and selected the best available insulating material, the insulation thickness is the only parameter which the designer can vary in order to seek an optimum. The following procedure can be used to find the optimum insulation.

In any zone the weight penalty can be written as

$$W_{PEN} = \mu \rho_{ins} A + \frac{\lambda}{L_E} \left[\frac{\beta A}{\delta} \int_o^{t_f} k(T_s - T_p) dt - \overline{\Delta H} \right] \qquad (21)$$

where μ = geometric factor for volume
ρ_{ins} = bulk insulation density
δ = the insulation thickness
k = the average thermal conductivity for the temperature range T_s to T_p.

The insulation thickness corresponding to a minimum penalty can be found by solving the equation

$$\frac{\partial W_{PEN}}{\partial \delta} = 0 \qquad (22)$$

Carrying out the differentiation, the equation which results is

$$\rho_{ins}\left[\mu+\delta\frac{\partial \mu}{\partial \delta}\right] + \frac{\lambda}{L_E\delta}\left[\left(\frac{\partial \beta}{\partial \delta} - \frac{\beta}{\delta}\right)\int_o^{t_f} k(T_s-T_p)dt + \frac{\beta}{\delta}\int_o^{t_f}\frac{\partial}{\partial \delta}k(T_s-T_p)dt\right] = 0 \qquad (23)$$

If the approximation

$$T_s = T_s^o = \left(\frac{I}{\eta\epsilon_o\sigma}\right)^{1/4} \qquad (24)$$

is used, then T_s is independent of δ, and the last integral in equation 35 vanishes. The equation then becomes

$$\rho_{ins}\left(\mu+\delta\frac{\mu}{\partial \delta}\right) + \frac{\lambda}{L_E\delta}\left[\frac{\partial \beta}{\partial \delta} - \frac{\beta}{\delta}\int_o^{t_f} k(T_s-T_p)dt\right] = 0 \qquad (25)$$

For design feasibility and for most performance analyses, further approximations may be made without introducing appreciable errors. The various geometric factors, μ,η,β are all functions of δ of the type

$$1 + a_1\left(\frac{\delta}{D}\right) + a_2\left(\frac{\delta}{D}\right)^2. \qquad (26)$$

For thin skins relative to tank diameter, δ/D is small, so then, the approximation

$$\eta,\beta,\mu = 1 \qquad (27)$$

is valid. In this case equation 25 can be further reduced to

$$\rho_{ins} - \frac{\lambda}{L_E \delta^2} \int_o^{t_f} k(T_s - T_p)dt = 0 \qquad (28)$$

or

$$\delta = \left[\frac{\lambda}{\rho_{ins} L_E} \int_o^{t_f} k(T_s - T_p)d\tau \right]^{1/2} \qquad (29)$$

The mass of the insulation is $\delta \rho_{ins} A$, so that the optimum insulation mass is

$$W_{ins}(opt.) = A \left[\frac{\rho_{ins} \lambda}{L_E} \int_o^{t_f} k(T_s - T_p)d\tau \right]^{1/2} \qquad (30)$$

In this form we see that the minimum payload penalty occurs when the weight of insulation is the product of λ times the weight of propellant boiled off due to the heat leak through the particular section of the tank being considered (see equations 9 and 21). The use of additional insulation to reduce boiloff below this amount will actually increase the payload penalty. This points out the error of setting a maximum allowable daily boiloff rate as the design objective.

For more accurate analyses, the first order terms in the geometric factors must be retained. In this case, the solution is more complex, but is still amenable to algebraic analysis.

5. Conclusions and Future Program

Based upon the material presented in this discussion we are of the opinion that the general principles for calculating an optimum insulating system for a propellant storage tank have been established. There is still a considerable amount of work which has to be done before this is worked out in its details. These efforts, however, are clearly delineated. They include the following:

1. The development of a general input analysis to define the thermal input to each section of the tank as a function of time and position in space. This part of the program has been held off until now in order to insure that its development would be consistent with the details of the analysis of which it will become a part.

2. Numerical studies to determine the accuracy and manipulative characteristics of the analytic techniques. An attempt to develop design methods along the "unit process" road will be made. This will be done through a systematic study of typical configurations by which correlations between heat leak, material properties and configuration may result.

3. Further refinement of analytic procedures. This will clude studies based on a novel simplified numerical analysis for heat transfer, the method of zones, which technique has been used on similar problems. There will also be an attempt to find approximate analytic solutions for cases where heat conductivity parallel to the skin is finite.

4. Studies of conduction in structural members. This program will consider the novel structural concepts to provide mechanical soundness and minimum heat leak, as well as determining heat leak in typical structural concepts used in the present generation of vehicles.

5. Experimental studies to provide precise, reliable information on the performance of thermal insulating materials. In particular, for radiation shielding, it is necessary to know the average thermal conductivity as a function of temperature difference and insulation thickness.

D. EXPERIMENTAL STUDY OF MULTILAYER RADIATION SHIELDING INSULATION

As was noted in our first quarterly report, we plan to conduct an experimental program to determine the influence of several variables on the average thermal conductivity of multiple layer insulations. The study we plan is concerned with determining the individual factors in the current shielding which limit their performance and assessing where improvements can be made. Knowing this we will then be in a position to recommend the directions that a materials development program should follow. In addition, it will provide data on the properties of current insulations. This data is needed for the detailed evaluation of any protective system. In this test program, we will undertake to determine:

1. Heat leaks due to residual gases.
2. Heat leaks due to spacers between shields.
3. Shield performance under external loads.
4. Shield performance as a function of temperature difference between the first and last shields.
5. Rate of evacuation to operational pressures.
6. The effect of the number and spacing of radiation shields upon their performance.

During the past quarter our effort has been devoted primarily to the design of the thermal conductivity apparatus which will be employed in this experimental program. Some features of this apparatus were indicated as concepts in the first quarterly report. These have now been worked out in detail. A meeting between Arthur D. Little, Inc. personnel and personnel of the National Bureau of Standards in Boulder, Colorado was held on March 14, 1961 and another meeting between Arthur D. Little, Inc. personnel and NASA personnel was held on March 16, 1961 to discuss the proposed design. The suggestions which were made during these meetings were incorporated into the final design. Detailed drawings of the components have been completed and the purchasing of necessary construction materials and construction of parts is underway.

We decided to use 300 series stainless steel throughout. Stainless steel presents advantages over other materials used at cryogenic temperatures:

a. Heli-arc welded construction, possible with the stainless steel, is more dependable at low temperatures and is usually free of vacuum leaks.
b. Heat leaks are low because of low thermal conductivity of stainless steel.
c. Stainless steel has high tensile strength.

Figure 2 shows the assembly drawing of the thermal conductivity apparatus. The apparatus is designed to work for twenty hours before cryogenic liquids have to be added.

Heat transfer calculations showed that the following vessel capacities are necessary:

a.	Outer liquid nitrogen vessel	36 liters
b.	Guard vessel	27 liters
c.	Measuring vessel	2.8 liters

Table III shows estimated maximum running time for insulations of different thermal conductivity and different thickness.

The plate sizes were chosen in accordance with ASTM recommendations for single guarded plate apparatus. The bottom of the measuring vessel, which constitutes the inner part of the cold plate, was chosen to be 6-inch diameter. The other dimensions are as follows:

Diameter of the guard vessel:	12 inches
Maximum thickness of the specimen:	2 inches
Gap between measuring and guard vessels:	1/8 inch
Surface planeness:	Not over .003 inches
Thermocouple size:	Not over 23 gage
Surface emissivity:	Over .8

The position of the lower (or warm) plate of the apparatus shown in Figure 2 is adjustable. This feature makes it possible:

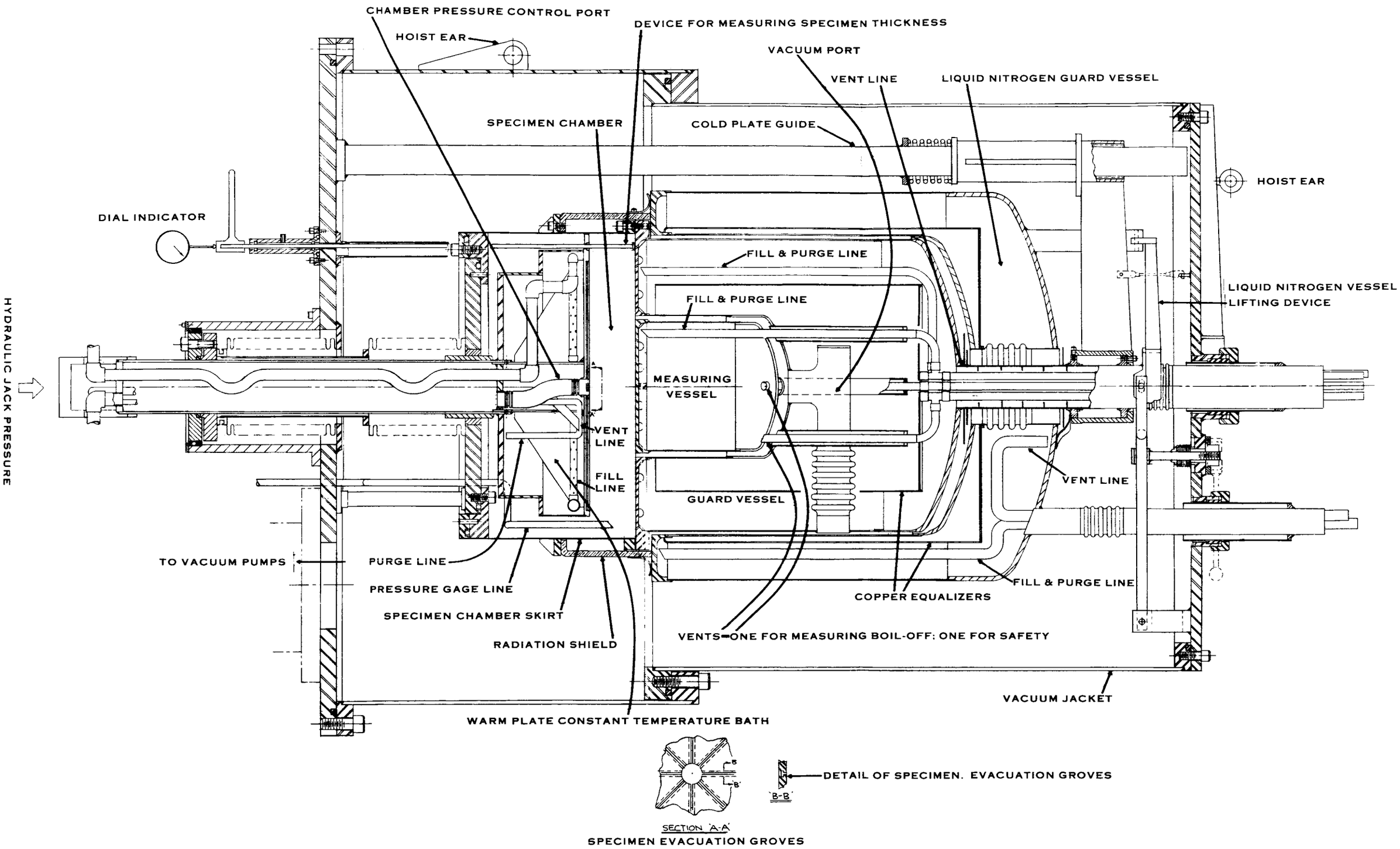

FIGURE 2

Assembly Drawing for the Thermal Conductivity Apparatus

TABLE III

MINIMUM INSULATION THICKNESS OF DIFFERENT INSULATIONS WHICH CAN BE TESTED IN THE THERMAL CONDUCTIVITY APPARATUS

Minimum Insulation Thickness L and Time in Which All Cryogenic Liquid Evaporates From Measuring Vessel

Liquid in Measuring Vessel	Solid K = 1 $\frac{\text{Btu in}}{\text{Ft}^2\text{HR}^\circ\text{F}}$	Foams, Powders K = 0.1	Evac. Powders K = 0.01	Multi Layer Insulation K = 0.001
Helium $T_2 = 4.2^\circ K$	--	--	L = 2" 14 Hr.	L = 1/4" 17 Hr.
Hydrogen $T_2 = 20^\circ K$	--	L = 2" 18 Hr.	L = 1/4" 22 Hr.	L = 1/8" 110 Hr.
Nitrogen $T_2 = 77^\circ K$	L = 2" 12 Hr.	L = 1/4" 14 Hr.	L = 1/8" 70 Hr.	L = 1/8" 700 Hr.

Warm Plate Temperature $T_1 = 300^\circ K$

a. to use a specimen of any thickness between 0 to 2 inches

b. to apply up to 50 psi pressure or to decrease the thickness of the specimen without interrupting the test

This feature will be important for investigation of the effect of mechanical loads on the insulation. The pressure will be applied hydraulically from the outside of the specimen chamber. During this operation the lower plate is guided by two teflon bushings 12 inches apart. Teflon is used for two purposes: 1) to provide smooth bearing, 2) to insulate the lower plate thermally from the base plate.

The lower plate covers a reservoir of 7 liters capacity. This reservoir can be filled with any cryogenic liquid, to keep the lower plate at constant temperature. Constant temperature water or oil flow could be channeled through this reservoir for the same purpose. If other temperatures between boiling points of cryogenic fluids and boiling points of water are required, cold or hot vapors can be sprayed through the provided nozzles. The constant temperature will be provided by the uniformly distributed sprays. Eight thermocouples embedded in the top surface of the lower plate measure the temperature.

The lower plate is equipped with eight 1/16 wide by 3/16 deep radial grooves and a 3/4-inch opening in the center (a total open area of less than 10% of the specimen surface) for more efficient evacuation of the specimen.

The specimen chamber is hermetically enclosed. Therefore, it is possible to evacuate the insulation specimen to any degree of vacuum or introduce different gases into the specimen without interfering with the main vacuum jacket surrounding the cryogenic vessels.

The lower plate can be removed from the apparatus for repair or modifications. The skirt which constitutes the side wall of the specimen chamber is also removable to make it possible to replace the

latter with other models if it should become desirable to do so. The upper part of the skirt is enclosed with a split copper ring which serves as a radiation shield at liquid nitrogen temperature and simultaneously a thermal short to the lower part of the skirt intercepting the heat leak from 300°K parts to the liquid hydrogen guard vessel. Before the final design of the measuring and guard vessels assembly was decided upon, the following components were analyzed:

a. The flat bottoms of the measuring and guard vessels constituting cold plate were chosen to be 1/4-inch thick reinforced by ribs. This assures the temperature of the lower surface of the plate to be less than 1/4°C above the boiling temperature of the cryogenic liquid.
b. The walls of the cryogenic vessels were checked for collapsing pressures. Thin walls are necessary to decrease the warm-up time and the amount of liquid required to cool the vessels down. (See Table IV.)
c. The tubes supporting the measuring vessel were checked for critical compression loads. Thin wall tubings are essential to decrease the possibility of the heat transport between measuring and guard vessels. Three 3/8 O.D. x .016-inch wall by 6-inch long tubes were found satisfactory.

We calculated that if the pressure at which the liquid nitrogen or hydrogen is normally boiling is changed by 1/2 psi, the boiling point of the gas will change by approximately 1/4°C for nitrogen and by 0.1°C for hydrogen. Calculations show that the pressure difference between guard and measuring vessels can be expected not to exceed 1/4 psi, thus making it possible to estimate the maximum expected heat transfer between the vessels for:

a. three 3/8-inch O.D. x .016-inch wall x 6-inch long tubes
b. residual gas conduction (at $P = 10^{-5}$ mm Hg)
c. radiation (gold plating is specified for the vessel walls)

TABLE IV

AMOUNT OF CRYOGENIC LIQUIDS REQUIRED TO COOL DOWN VESSELS FROM ROOM TO OPERATING TEMPERATURES

Vessel	Oper. Temp. (°K)	Weight of Vessel (Lbs.)	Heat Required (BTU)	Cryog. Liq. Required (Liters)
Measuring Vessel	20°	4.3	188	6.2 - LH_2
Guard Vessel	20°	33	1440	47.5 - LH_2
Liquid Nitrogen Vessel	77°	60	2240	15 - LH_2

It was found that this heat transfer could present an inaccuracy in the measurement of about 10% of the total expected heat transfer through the test specimen. This can be reduced to 1% by reducing the pressure to 10^{-6} mm Hg and the gas pressure difference between the vessels to one inch of water column.

Pressure drops through vent lines of measuring and guard vessels were calculated and found to be less than .005 psi (approximately .12-inch W.C.). The measuring vessel is supplied with a separate relief line in case the other two lines should become plugged. Since the guard vessel vent line is of much larger diameter, we did not feel it necessary to provide a separate relief line for the guard vessel.

All four vessels: measuring, guard, liquid nitrogen and warm plate are supplied with fill lines which serve simultaneously as purge lines when it is necessary to remove the cryogenic fluids. This arrangement will save time during warm-up period.

Guard and nitrogen vessels have copper shields (see Figure 2) which serve as temperature equalizers and radiation shields during the time when liquid level is low.

The liquid nitrogen vessel can be lifted and lowered by 1/4-inch without interrupting the test. This allows breaking the thermal contact between the liquid nitrogen vessel and copper radiation shield attached to specimen chamber skirt, making it possible to change its temperature distribution. Extreme caution was exercised to make all components accessible and removable for repair and to achieve flexibility of the entire apparatus.

During the next quarter we expect to assemble the apparatus, the vacuum pumping system, mounting cabinet and hoist arrangement for lifting the components. Preliminary tests on the apparatus will be carried out at liquid nitrogen temperatures.

III. INTERACTIONS WITH THE METEOROID ENVIRONMENT

A. THE EVALUATION OF METEOR BUMPERS

1. First Order Theory

In 1946 Whipple suggested that a thin shield or "bumper" spaced some distance from the pressure hull of a space vehicle would cause meteoroids hitting it to disintegrate, thus preventing their doing damage to the main structure of the ship (9). Subsequently, a number of experimenters have observed that pellets of various types fired at thin targets broke up into small pieces and did relatively little damage to a second target some distance behind the first (10,11). These experimental observations are a confirmation of Whipple's initial suggestion. However, this is only the first step in obtaining the information which an engineer will require to design a suitable bumper for protecting space vehicles against meteoroids. The following analysis was the first attempt to obtain an appreciation of the physics of the performance of a meteoroid bumper. The model which was chosen is based on the following assumptions:

1. The pellet or projectile velocity, V_1, is large compared to the acoustic velocity in the pellet or bumper material.
2. The dimensions of the pellet are large compared to the thickness of the bumper.
3. After breakup by the bumper, the energy of the resulting system may be given by the sum of two terms, namely (a) the kinetic energy of motion relative to the center of mass of the system, plus (b) the kinetic energy of the center of mass of the particles. Thus, it is assumed that the energy dissipated as heat, light, etc. is small in comparison to that which goes into the motion of the particles relative to the center of mass.

4. The mass of material passing through the bumper breaks up with spherical symmetry about the center of mass. For the purpose of an initial analysis, this assumption is a convenient compromise among the range of possible distributions of fragments about the center of mass.

Figure 3 shows the pellet-bumper interaction. Based upon this picture, and the assumptions given above, we may state the following:

$$m_1 V_1 = (m_1 + m_2)\, V_2 \quad \text{(conservation of momentum)} \tag{31}$$

$$m_1 V_1^2 = (m_1 + m_2)\, V_2^2 + (m_1 + m_2)\, V_3^2 \quad \text{(conservation of energy)} \tag{32}$$

where m_1 = initial projectile mass

m_2 = mass of shield material intercepted by the projectile

V_1 = initial projectile velocity

V_2 = velocity of center of mass of $m_1 + m_2$ after the collision

V_3 = energy average velocity of particles relative to center of mass.

If m_1, m_2 and V_1 are known, equations 31 and 32 can be solved for the ratio V_3/V_2, i.e.

$$V_3/V_2 = (m_2/m_1)^{1/2} \tag{33}$$

The half angle of the spray of fragments is simply

$$\theta = \sin^{-1}(1.28\, V_3/V_2) = \sin^{-1}\left[1.28\, (m_2/m_1)^{1/2}\right] \tag{34}$$

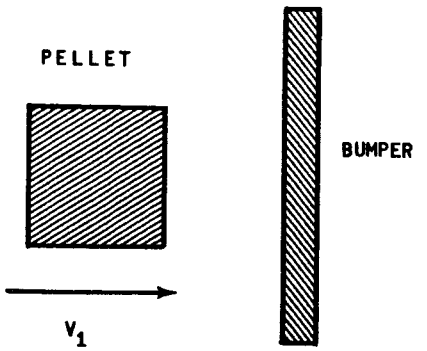

a. Prior to Impact

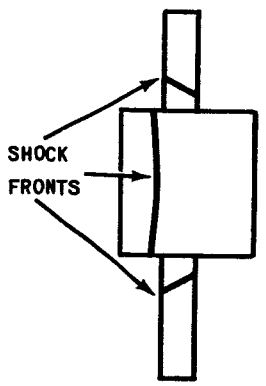

b. During Impact

$\alpha = \text{TAN}^{-1} \frac{V_3}{V_2}$ = SPRAY HALF ANGLE

V_2 = VELOCITY OF CENTER OF MASS (C.M.)

V_3 = MAXIMUM VELOCITY RELATIVE TO C.M.

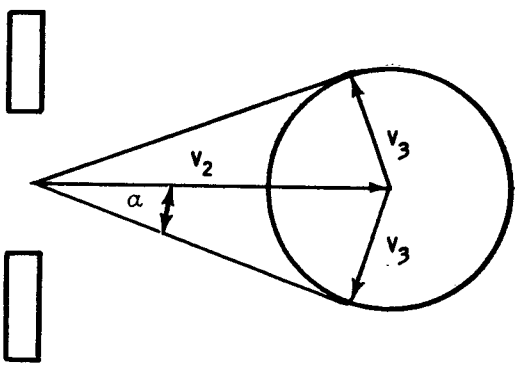

c. Expanding Spherical Particle Cloud After Impact

FIGURE 3 | Model for Pellet-Bumper Interaction

where the constant 1.28 is the ratio of the velocity of the outside of the exploding sphere of fragments to the average particle velocity away from the center of mass for the case where the density of the exploding particle is uniform. The curve for this relation is plotted in Figure 4 along with the results of some of the experiments described in the next section.

It should be noted that in equation 34, it is predicted that the angle θ is independent of the initial velocity of the projectile. This is due to the assumption that the energy dissipated in rupturing the bumper and the projectile is but a small fraction of the total energy which is dissipated.

$$\text{i.e.} \quad \frac{m_1 m_2}{m_1 + m_2} V_1^2 \ggg E_R \tag{35}$$

where E_R is the work that must be done to fragment the particles.

It should also be noted that if the energy which is dissipated in heat and light is a constant fraction of the total dissipated energy, it would be necessary to introduce a multiplying factor in equation 34, i.e.

$$\theta = \sin^{-1} \left[1.28 \, K^{1/2} \, (m_2/m_1)^{1/2} \right] \tag{36}$$

where K is the fraction of the dissipated energy which is converted into the motion of the particles relative to the center of mass.

2. Hypervelocity Tests Against Bumper-Type Targets

a. Avco Tests

Mr. Stephen Georgiev at Avco Research Company has been studying re-entry ballistics with a 22-caliber constant volume gun of his own design. He took an interest in our concepts concerning the interaction

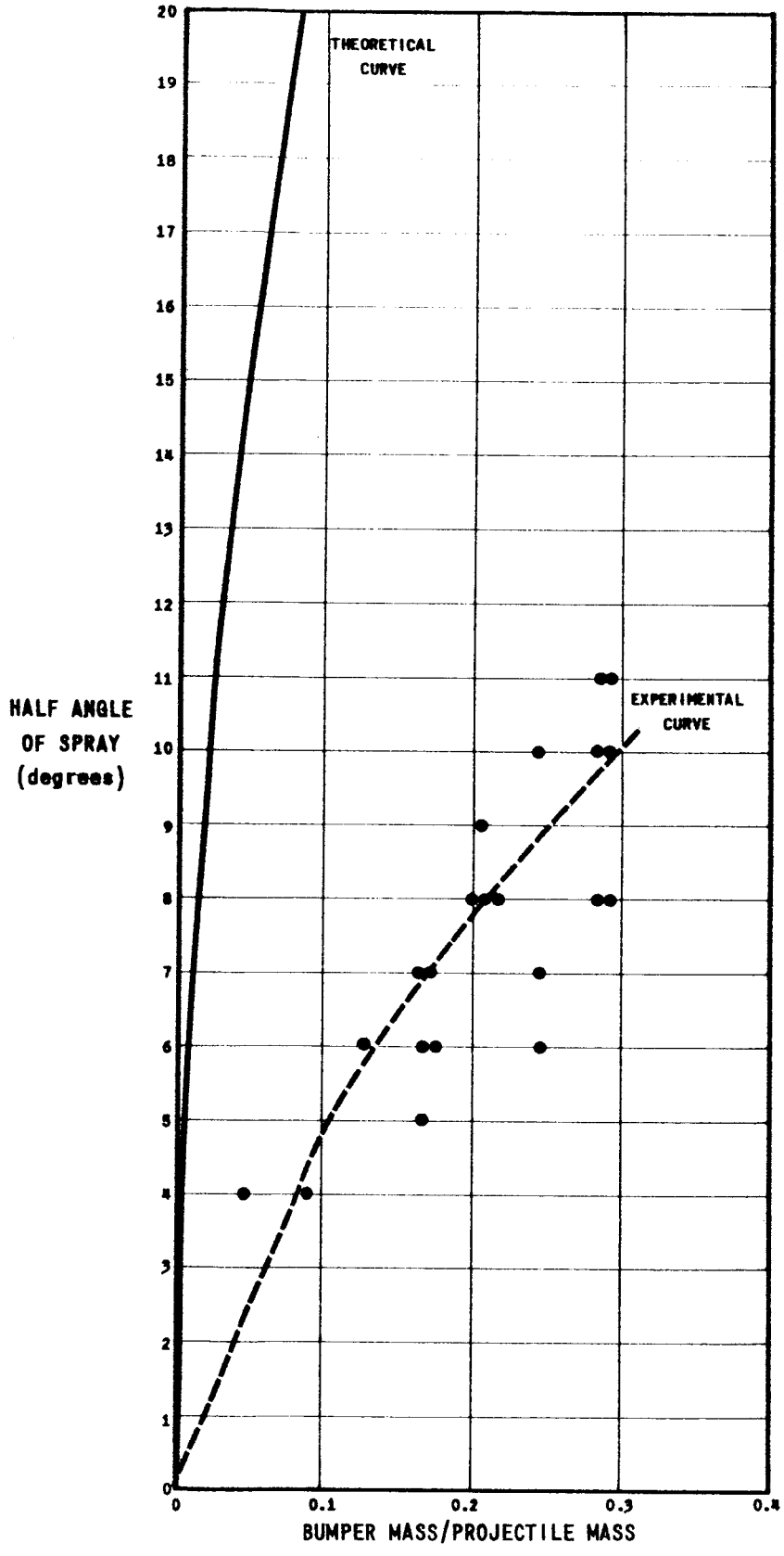

FIGURE 4 | Fragment Spray Angle vs Ratio of Bumper to Projectile Mass

of projectiles with thin targets and offered to place targets at the end of his range and then loan them to us for our evaluation.

To date he has impacted 68 bumper-type targets placed 2 3/4" in front of witness plates. The missile in all cases was a nylon sphere. Velocities have ranged up to about 18,000 ft/sec.

The damage to the bumper in general consists of a clean round hole. Typical damage to several witness plates is shown in Figures 5 to 8.

One expects the spray formed by a sphere hitting the bumper in a vertical trajectory to be circular and in general the patterns on witness plates confirm this. However, in many instances the patterns are somewhat unsymmetrical giving rise to a suspicion that the spheres were distorted.

The half angle of the spray was plotted against the bumper mass per unit area for several bumper materials and velocities. Figure 4 indicates a correlation although there is a great deal of spread in the observed spray angle for bumpers of the same density.

In Figure 9 the half angle of spray is plotted against velocity of impact for one bumper thickness and material. Here again, there appears to be a correlation. The spray angle appears to increase rapidly with velocity over the range of the experiments.

b. Lincoln Laboratory

The Lincoln Laboratory has recently completed an aeroballistic range for studying re-entry physics. They are firing 1/4" diameter aluminum spheres at velocities up to 20,000 ft/sec. Dr. Melvin Herlin and Mr. Richard Slattery agreed to place some targets furnished by us in their range to stop the projectiles after they have made their measurements. These tests are run on a non-interference basis at no charge.

c. Data from CARDE

A visit was made to Dr. Gerald Bull and Mr. George Tidy at the Canadian Armament Research Defence Establishment at Valcartier, Quebec.

FIGURES 5-8

THE EFFECT OF BUMPERS

PHYSICAL DATA FOR ALL SHOTS

Missile = 0.218" diameter Nylon Sphere
Velocity = 17,000 - 18,000 ft/sec
Bumper Standoff = 2.75"
Avco, December 1960

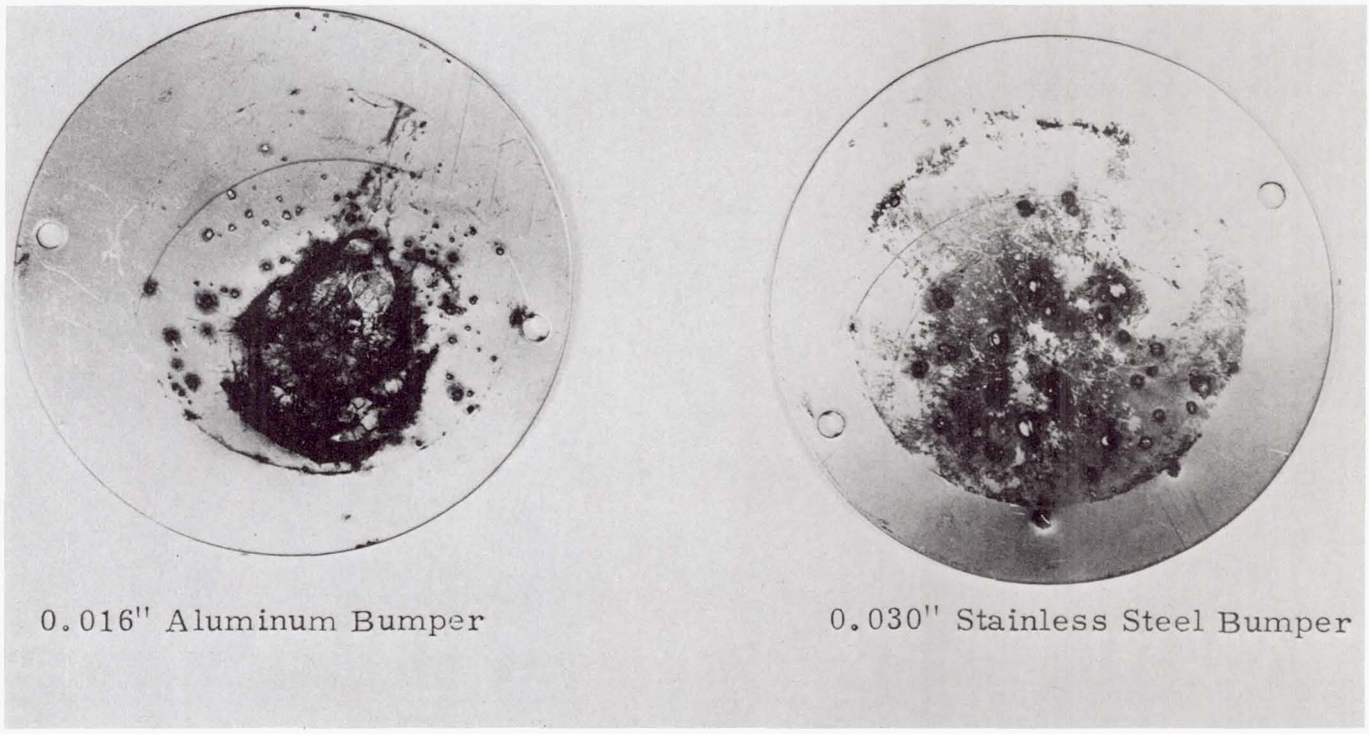

FIGURE 5 | Damage to Witness Plates Behind Metal Bumpers

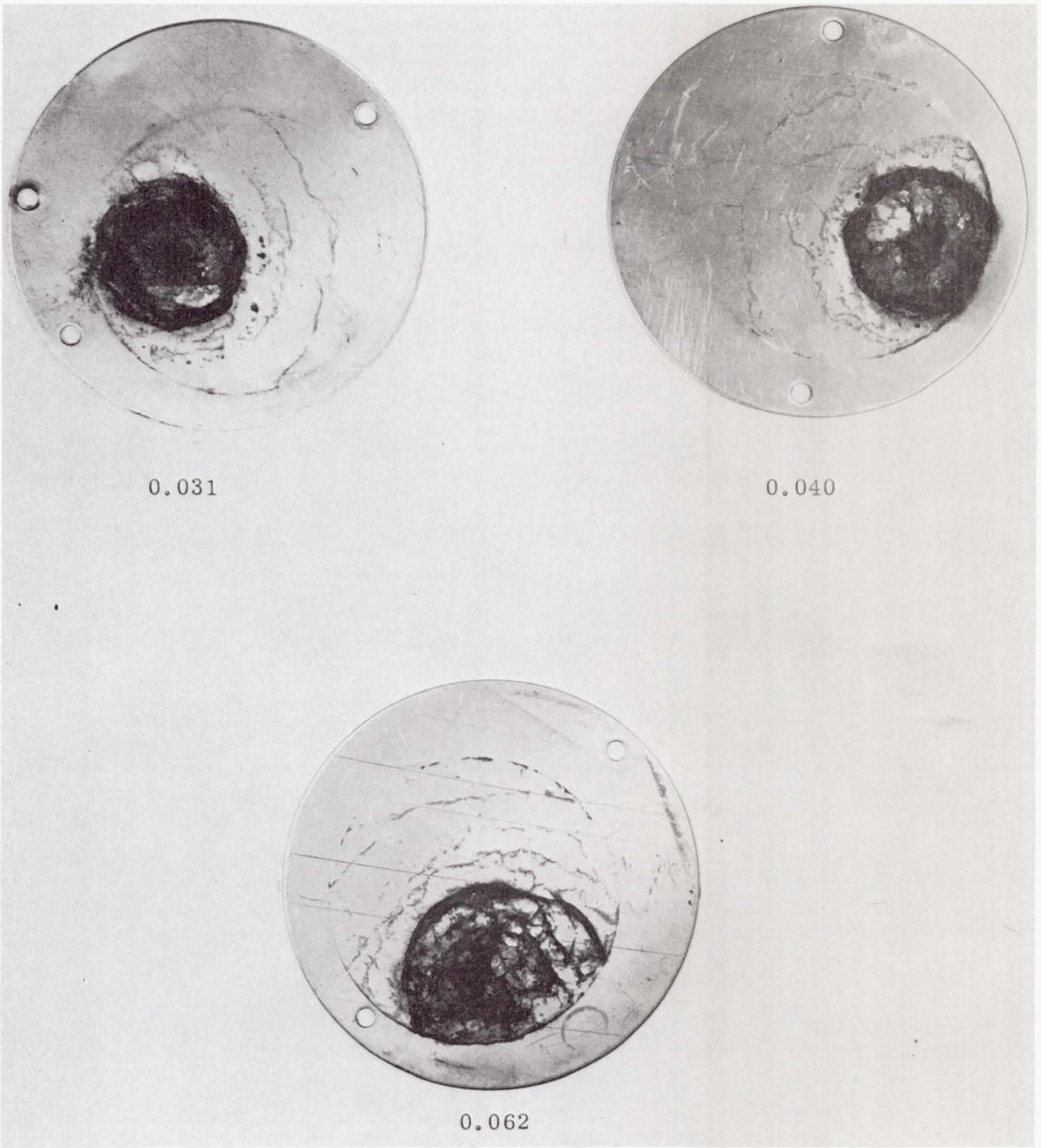

FIGURE 6 | Damage to Witness Plates Behind Nylon Bumpers

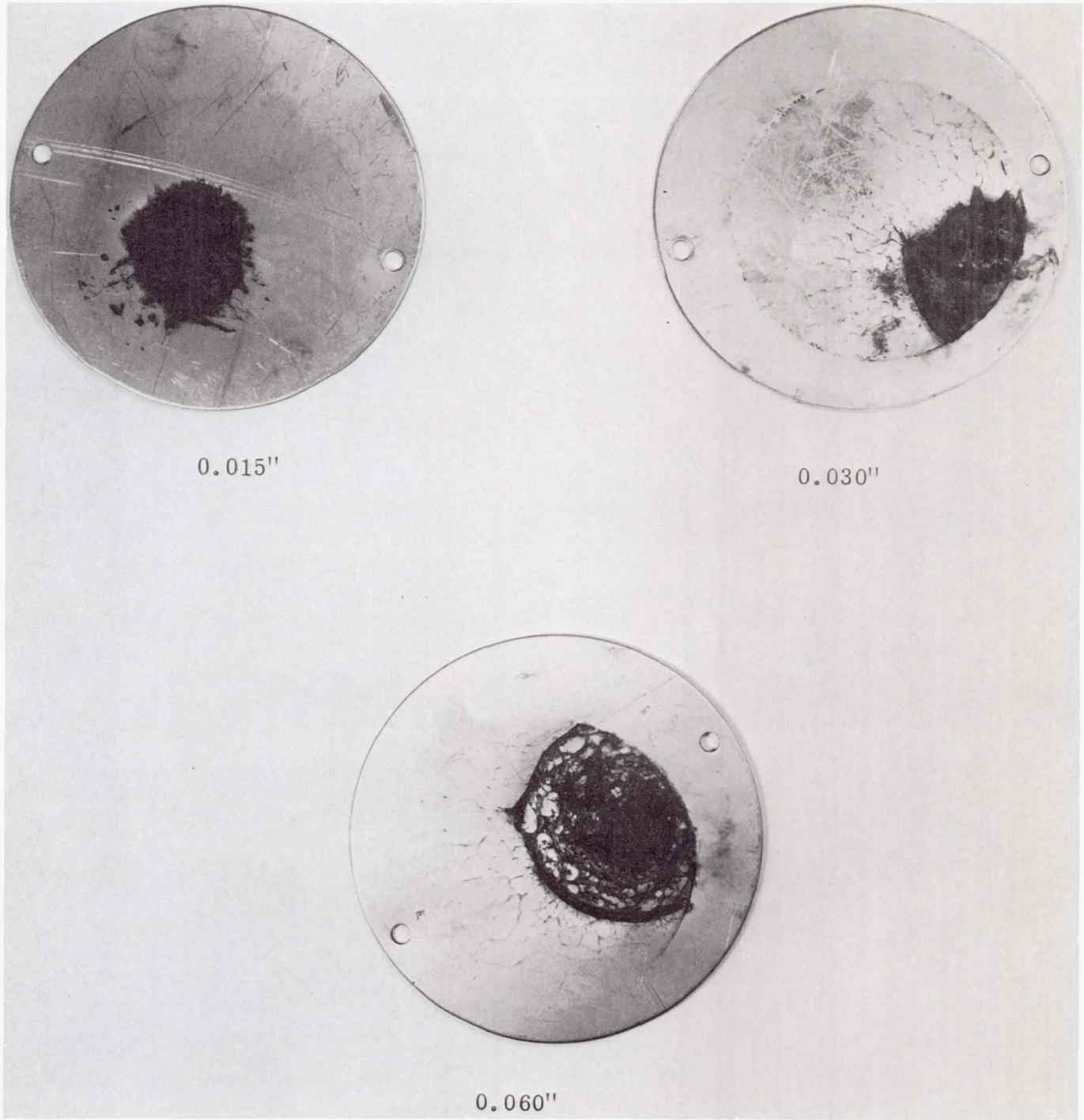

FIGURE 7 | Damage to Witness Plates Behind Polyethylene Bumpers

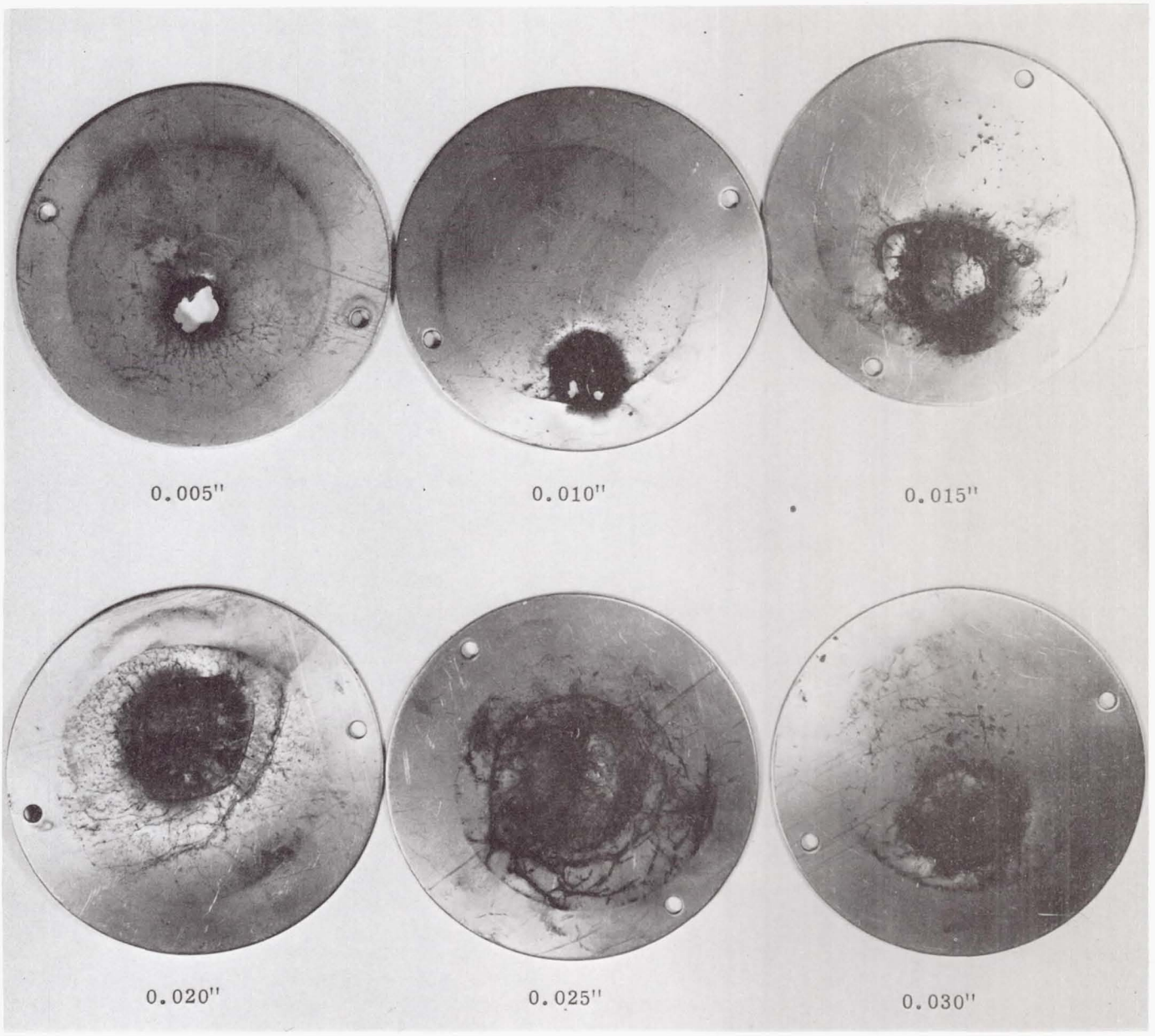

FIGURE 8 | Damage to Witness Plates Behind Bumpers of Laminated 5 Mil MYLAR

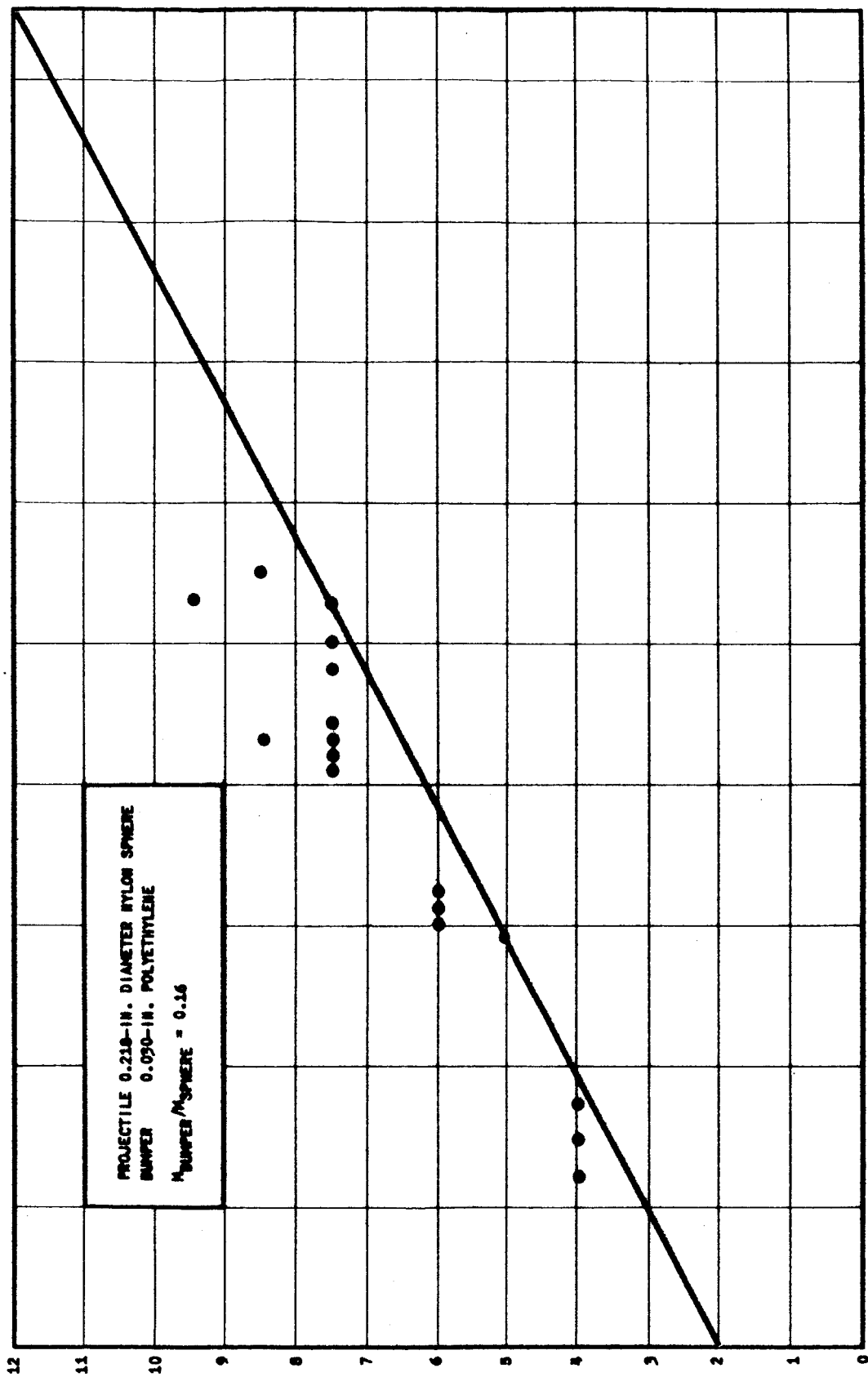

FIGURE 9 Fragment Spray Angle vs Projectile Velocity

They had fired a series of magnesium and aluminum slugs at 1/8" steel bumpers and observed quite unsymmetrical spray patterns on steel witness plates.

On March 20 and 21, Dr. Bull visited us on a consulting basis. When he returned to CARDE he made a series of four tests in which the velocity was varied. In these shots a 5/8" thick aluminum witness plate was mounted one foot behind a 20 mil aluminum bumper. The projectile was a plastic cylinder 0.55" in diameter by 0.35" long and weighed 1.6 grams. In all of these shots the trajectory was normal to the bumper and witness plate. One shot was at 14,000 ft/sec, one at 16,000 ft/sec and two at 20,000 ft/sec. At 14,000 ft/sec the projectile hit the bumper with its cylindrical axis parallel to the bumper face and penetrated both bumper and witness plate. At 16,000 ft/sec the projectile axis was perpendicular to the bumper and also penetrated both the bumper and witness plate. At 20,000 ft/sec the projectiles were cocked at an angle of 45° when they impacted the bumpers. Both shots gave identical damage patterns. A witness plate for one of these shots is shown in Figure 10.

The sharp outline of the damage, the smooth curves of its edges, the bilateral symmetry and internal detail and the reproducibility all indicate that the breakup of the pellet is an orderly process capable of analysis and description. It is apparent that for a very thin bumper the shape of the pellet and its orientation at impact are very important in determining how it breaks up.

The sharply defined circular craters in the upper left and lower right part of the picture are all made by fragments of aluminum pushed out of the bumper. The dense group of craters at the lower right were made by bumper fragments accelerated by the flat face of the pellet. The arc of craters at the upper left was formed by fragments accelerated by the cylindrical surface of the pellet.

It would appear that the pellet itself was acted upon by a very strong plane shock induced in the flat face of the pellet by its interaction with the bumper and by a converging conical (nearly cylindrical) shock similarly induced in the cylindrical surface of the pellet.

FIGURE 10 | Witness Plate for Carde Shot

The plane shock sheared a large ring off the periphery of the pellet. The converging shock generated a jet from the top or rear face of the pellet.

3. Test Results and Comparison with Theory

Data obtained by Arnold Olshaker at M.I.T. (11) who fired lead spheres into lead targets at velocities of the order of 8-9000 ft/sec fell very close to the theoretical curve calculated from equation 34 and shown in Figure 4. The other data obtained in the tests described above for plastic and aluminum projectiles do not fall on the theoretical curve. In all these tests the observed spray angles are much smaller than predicted. The small spray angles may be due to any of the following reasons:

a. An appreciable fraction of the initial projectile kinetic energy is consumed in breaking up the projectile and the bumper material. This would imply that larger angles would occur with increasing projectile velocity. This effect was observed. (Figure 9).

b. An appreciable fraction of the total energy which is dissipated goes into heat, light and other dissipative phenomena. Although we know that some of the energy is consumed in this manner, we have no direct measure of its magnitude, beyond the fact that the experimental data can be fit reasonably well by using a value of 0.1 for K in equation 36. This would imply that as much as 90 per cent of the dissipated energy goes into such processes. This, of course, is a maximum estimate and assumes that all deviations from theory are due to this mechanism, which is probably not true.

c. The breakup of the projectile and bumper is not spherical but rather is elongated in the direction flight. This effect has been observed and is clearly

indicated by the data obtained at CARDE. (Figure 10). If the breakup tends to be one dimensional, then the shape of the pellet and its orientation at impact will have a large effect on the distribution of particles in the spray.

The major implication of these results is that before it will be possible to assess the usefulness of meteor bumpers as protective devices for space vehicles more must be known about the mechanism whereby the particles break up. Empirical data will be of immediate value to the design engineer who is now concerned with the design of such bumpers. In the long run, however, we are of the opinion that it would be desirable to have a detailed understanding of the physics of the phenomenon. Thus our continuing effort is concerned with generating both types of information.

The experimental program will be concerned with obtaining bumper performance characteristics as a function of projectile and bumper material and dimensions, projectile velocity and distance between the bumper and witness plate. In this regard, it should be noted that there are appreciable experimental efforts currently underway at the Ames and Langley Research Centers of NASA and at the Ballistics Research Laboratories. This work will provide much of the needed empirical information, and we do not plan to duplicate it. Instead our concern will be to perform additional tests which seem advisable. In addition, we do plan to undertake a basic study of the physics of the breakup. The direction this will take is indicated by the initial analysis which is described in the next section.

B. THE IMPACT OF PELLETS WITH THIN PLATES

1. Description of the Model

A pellet impacting and passing through a thin plate at high velocities, will have propagated through it a shock wave which, depending on the impact conditions, will tend to shatter the pellet and cause the residue to form a growing cloud of small particles. In sorting out the physics of the problem it is necessary to establish a basic model of the processes occurring. In general the problem is one of non-stationary wave propagation, and has many analogies with shock-tube processes. In particular, if the transmitted impact shocks are sufficiently strong, the materials will become fluid, and the basic shock-tube analysis can be applied. The intermediate cases, where rather non-homogeneous particle clouds are developed is considerably more complex, and discussion in this memorandum will be confined to the case where fluid flow conditions may be assumed. The interesting theoretical condition discussed by Stanyukovich (15), whereby most materials follow the isentropic law $P = A\rho^{\gamma}$ to rather extremely large pressures is applicable in this case.

The basic initial parameters are pellet characteristics and velocity, ρ_{p_o}, P_{p_o}, T_{p_o}, V, and bumper plate characteristics ρ_{B_o}, P_{B_o}, T_{B_o}, and δ (as shown in Figure 11). For simplicity a simple end-on cylindrical impact is assumed; the complex problems of varying shape and impact angle requires consideration beyond the scope of this discussion.

The postulated wave model is shown in Figure 11; basic to this approach is the requirement that the bumper plate be extremely thin; the geometry of Figure 11 is exaggerated to show detail. For sufficiently thin bumper plates, one dimensional wave motion during transmission through the bumper is a reasonably valid assumption (12).

Impact is assumed to occur at time, t = o. On impact a shock wave $\xrightarrow{S_B}$ travels forward through the bumper plate, inducing a particle velocity, u_B, behind it in the direction of travel of the shock. A reflected shock wave is transmitted through the pellet, $\xleftarrow{S_P}$, decreasing

A. NOTATION

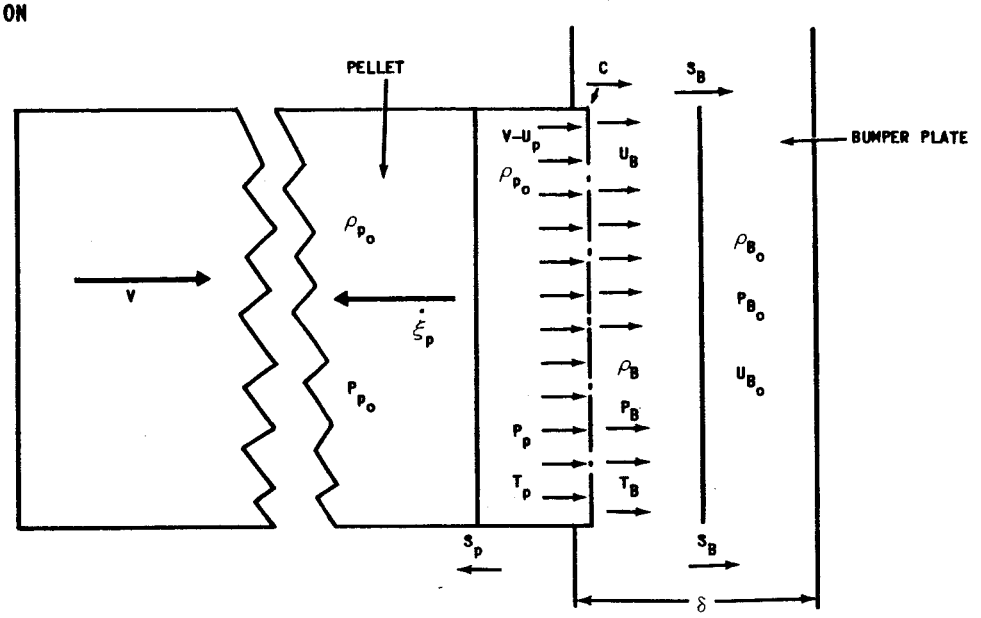

B. CHARACTERISTIC DIAGRAM FOR $V < \dot{\xi}_p$

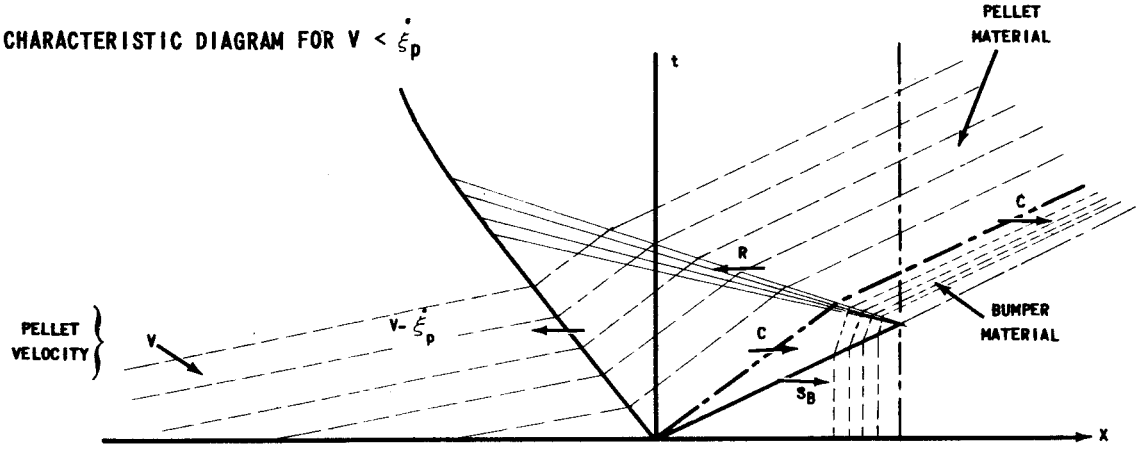

C. CHARACTERISTIC DIAGRAM FOR $V > \dot{\xi}_p$

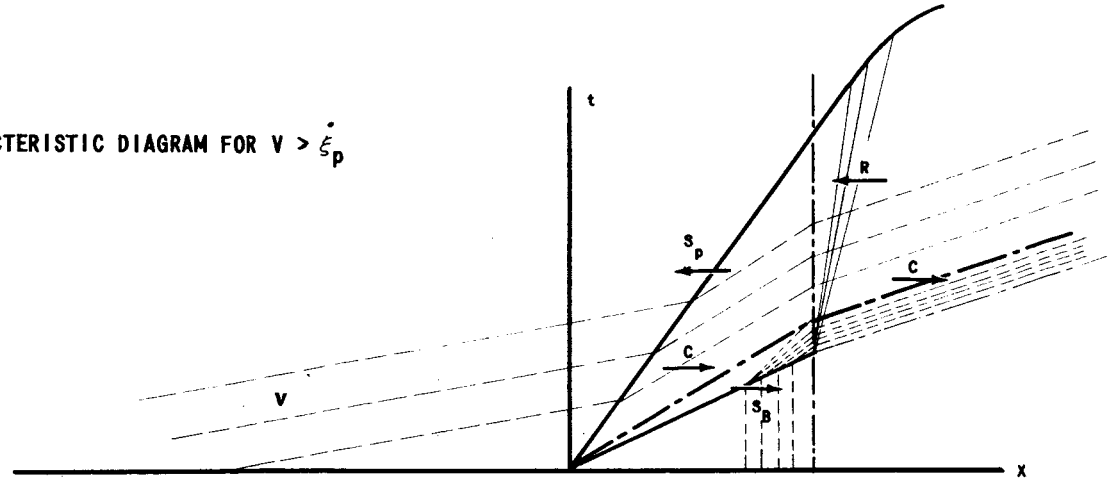

FIGURE 11 | Impact Wave Diagrams

the pellet particle velocity by an amount u_p, such that a contact surface C, separating bumper and pellet material, exists, i.e. $u_B = V - u_p$. When $\xrightarrow{S_B}$ reaches the far surface of the bumper plate it is reflected as a rarefaction (the stopping shocks discussed in references 15 and 16, increasing u_B and decreasing u_p as it proceeds through the pellet. Two cases are illustrated in Figure 11; in the first the pellet translational velocity V is less than the shock velocity, so that with respect to the fixed axis system, the shock proceeds upstream through the pellet from the point of impact. In this case if this reflected shock was sufficiently strong to break the pellet, the end opposite impact would be broken before reaching the plate. In the second case the pellet velocity is greater than the shock velocity, and the far end of the pellet passes well downstream of the impact point before being affected by the reflected shock.

This one-dimensional picture should be adequate to describe conditions shortly after impact; i.e., to derive initial impact shock strengths, etc. Thus, the pellet has transmitted through it in a direction opposite to its travel a pressure pulse whose duration in a one-dimensional concept is from passage of the reflected impact shock to the passage of the stopping rarefaction. However, since the pellet surfaces are free, a cylindrical rarefaction will travel inwards during the time any excess pressure exists between the pellet and its surroundings, inducing a radial outflow. This is illustrated in Figure 12; in 12a the one-dimensional picture is shown, whereas in 12b the more realistic three-dimensional system is shown. The shock is strongly attenuated by these inward facing rarefactions and becomes curved. The pellet particles develop a radial outward velocity component, which can be calculated

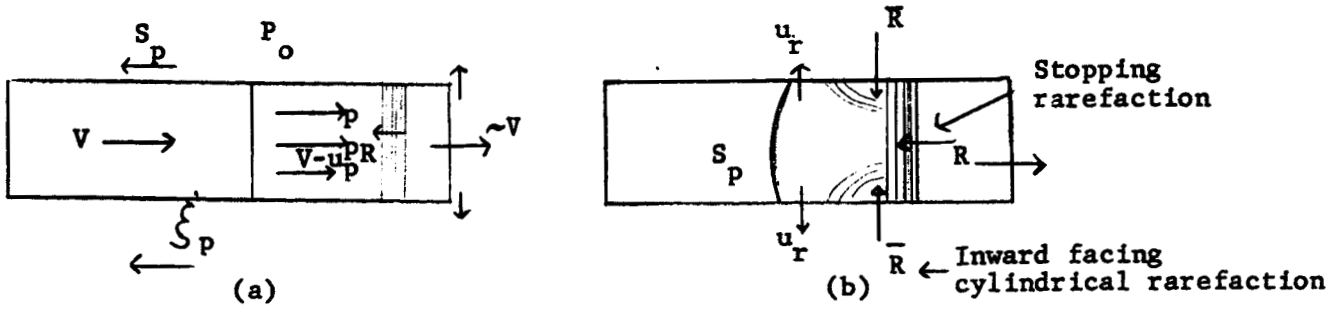

Initial Impact Shock Schematic

Figure 12

knowing the thermodynamic properties of the flow. If the pellet is long enough, the attenuation will ultimately transform the shock into a weak elastic wave.

2. Strength of the Impact Shock

On impact, the initial shock conditions are shown enlarged in Figure 13.

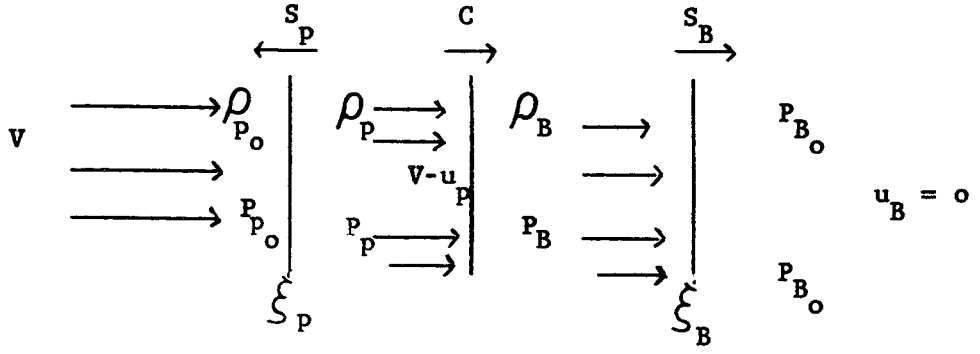

Initial Shock Conditions

Figure 13

The mechanical shock conditions may be written for this case:

$$\rho_{p_o} (\dot{\xi}_p + V) = \rho_p (\dot{\xi}_p + V - u_p) \tag{37}$$

$$P_{p_o} + \rho_{p_o} (\dot{\xi}_p + V)^2 = P_p + \rho_p (\dot{\xi}_p + V - u_p)^2 \tag{38}$$

$$\rho_{B_o} \dot{\xi}_B = \rho_B (\dot{\xi}_B - u_B) \tag{39}$$

$$P_{B_o} + \rho_{B_o} \dot{\xi}^2_B = P_B + \rho_B (\dot{\xi}_B - u_B)^2 \tag{40}$$

where across the contact surface separating bumper plate and pellet material:

$$V - u_p = u_B \tag{41}$$

$$P_p = P_B \tag{42}$$

The known parameters all refer to the unshocked states (i.e., ρ_{B_o}, P_{B_o}, ρ_{p_o}, P_{p_o}) and the pellet striking velocity V. It remains to determine the seven unknowns P_p, ρ_p, μ_p, ρ_B, μ_B. $\dot{\xi}_p$ and $\dot{\xi}_B$. Equations (37) to (42) must be augmented by another expression if these unknowns are to be determined. This should be an equation of state to take into consideration the thermodynamics of the process. If entropy effects are negligible, a Bridgman form of the equation of state may be used. (See Pack et.al. (17) in their investigation of explosively induced shocks in lead and steel).

$$1-\rho_o/\rho = \frac{3}{a\beta} P - \frac{3}{2a^2\beta^2} (\beta + 6)^2 \tag{43}$$

where a and β are parameters by means of which extrapolation to high pressures can be made from low pressure results on hydrostatic compression. This may be written in alternate forms:

$$P = A\rho^{\gamma} - B \tag{44}$$

or possibly for certain limiting conditions:

$$P = A\rho^{\gamma} \tag{45}$$

With the model assumed, some interesting observations follow directly from symmetry. If bumper and pellet are the same material, then S_B and S_p are $\xrightarrow{\quad}$ $\xleftarrow{\quad}$

identical but opposite facing shocks and from equation (41)

$$u_B = u_p = 1/2\ V \tag{46}$$

That is, the initial impact shock decelerates the shocked pellet material to one half its striking velocity and accelerates the bumper plate to this same velocity. The reflected rarefaction then accelerates the material to its final velocity. The above equations are considerably simplified in this case and by proper arrangement expressions can be obtained for wave velocity, shock strength, etc.

3. The Particle Cloud

The shape of the particle cloud behind the bumper must be derived from a solution of the complete wave system in the pellet and no obvious approximations appear that would yield simple expressions for the conical angle of cloud growth. Indeed, it would appear that the assumption of a conical cloud may not be realistic. The induced axial velocities will tend to lengthen the pellet, and it is to be expected that maximum induced radial velocity will occur at the impact end of the pellet. If the pellet is long enough, the shock would be completely attenuated before reaching the far end of the pellet, and an inverted cone might appear.

4. Future Work

It is our opinion that the preliminary work discussed in this section warrants further investigation. It is our intent to pursue the theoretical solution to the point where it will be possible to describe the breakup of the projectile and the intercepted portion of the bumper in terms of the material parameters and the velocity of the projectile. We also plan, where possible, to check the major premises and conclusions of this work by simple, directed experiments.

C. OTHER PROTECTION SYSTEMS

At the present time there seems to be but two reasonable approaches to a protection system against meteors - either the wall of the vehicle is made sufficiently thick so that the probability of a penetration during a space voyage is small or a "meteor bumper" is used. A primary part of our program has been an investigation of the meteor bumper effectiveness and its design criteria. However, we are also concerned with seeking other possible protection systems. It has been suggested that it should be possible to detect meteoroids while they are distant from the vehicle. Then either a movable bumper would be placed in the path of the meteoroid or the vehicle would be moved out of its path (18,19). It would appear pertinent to determine whether such an approach is feasible. This may be done by evaluating the time-distance relationships for such a system assuming that a meteoroid sensor could be constructed. With this in mind we have investigated the possibility of detecting meteoroids by optical means.

A spherical particle with a perfectly diffusing surface obeying Lambert's law, when illuminated in full phase will reflect in the direction of the observer 2/3 as much light as would a flat surface of the same angular subtense. Thus the intensity of radiation from the particle in the direction of the observer may be given as $2/3\ I_o R^2$, where R is the particle radius, and I_o is the intensity of the radiation incident upon the particle. The illumination at an observation point a distance, D, from the particle will be $2/3\ I_o (R/D)^2$, if the particle is observed in full face. In general, the particle will be observed at a phase angle θ, defined as the angle between the direction to the sun and the line of sight. The factor describing the dependence of luminous intensity on phase angle for a perfectly diffusing sphere is $\frac{1}{\pi}\left[\sin\theta + (\pi-\theta)\cos\theta\right]$. This factor is unity for $\theta = 0$; $\frac{1}{\pi}$ for $\theta = \pi/2$; and 0 for $\theta = \pi$. Thus the expression for the intensity at the observer, I, is

$$I = \frac{2}{3\pi} I_o \left[\sin\theta + (\pi-\theta)\cos\theta\right]\left[R/D\right]^2 \qquad (47)$$

For comparative purposes it is convenient to introduce the quantity, stellar magnitude, since the particle will be seen as a bright point against the star background. If it is to be detected its brightness should be comparable with that of the stars. Thus it is convenient to use the standard unit of stellar brightness. The apparent stellar magnitude, m, is defined as

$$m = -2.5 \log I + m_o \tag{48}$$

where m_o is a constant. m_o can be determined by using the apparent stellar magnitude of the sun as a standard. This is -26.7 at the earth's distance from the sun. Thus, if I_s is the illumination of the sun at the earth,

$$m_o = -26.7 + 2.5 \log I_s \tag{49}$$

Also, since the particle which is being observed is illuminated by the sun, I_o may be given in terms of I_s, namely

$$I_o = I_s/L^2 \tag{50}$$

where L is the distance from the sun in A.U. By combining equations (47) to (50), we can write an expression for the stellar magnitude of the meteoroid as a function of its radius, R, its distance from the observer, D, its phase angle, θ, and its distance from the sun, L, i.e.

$$m = -25.0 + 5 \log L - 5 \log f(\theta) - 5 \log (R/D) \tag{51}$$

where

$$f(\theta) = \left[\sin \theta + (\pi-\theta) \cos \theta\right]^{1/2} \tag{52}$$

Figure 14 is a plot of stellar magnitude versus distance from the vehicle, D, for particles of various sizes. These curves are calculated for L = 1; i.e., the vehicle is at 1A.U. from the sun. For comparative purposes, it may be noted that the stars visible with the naked eye have

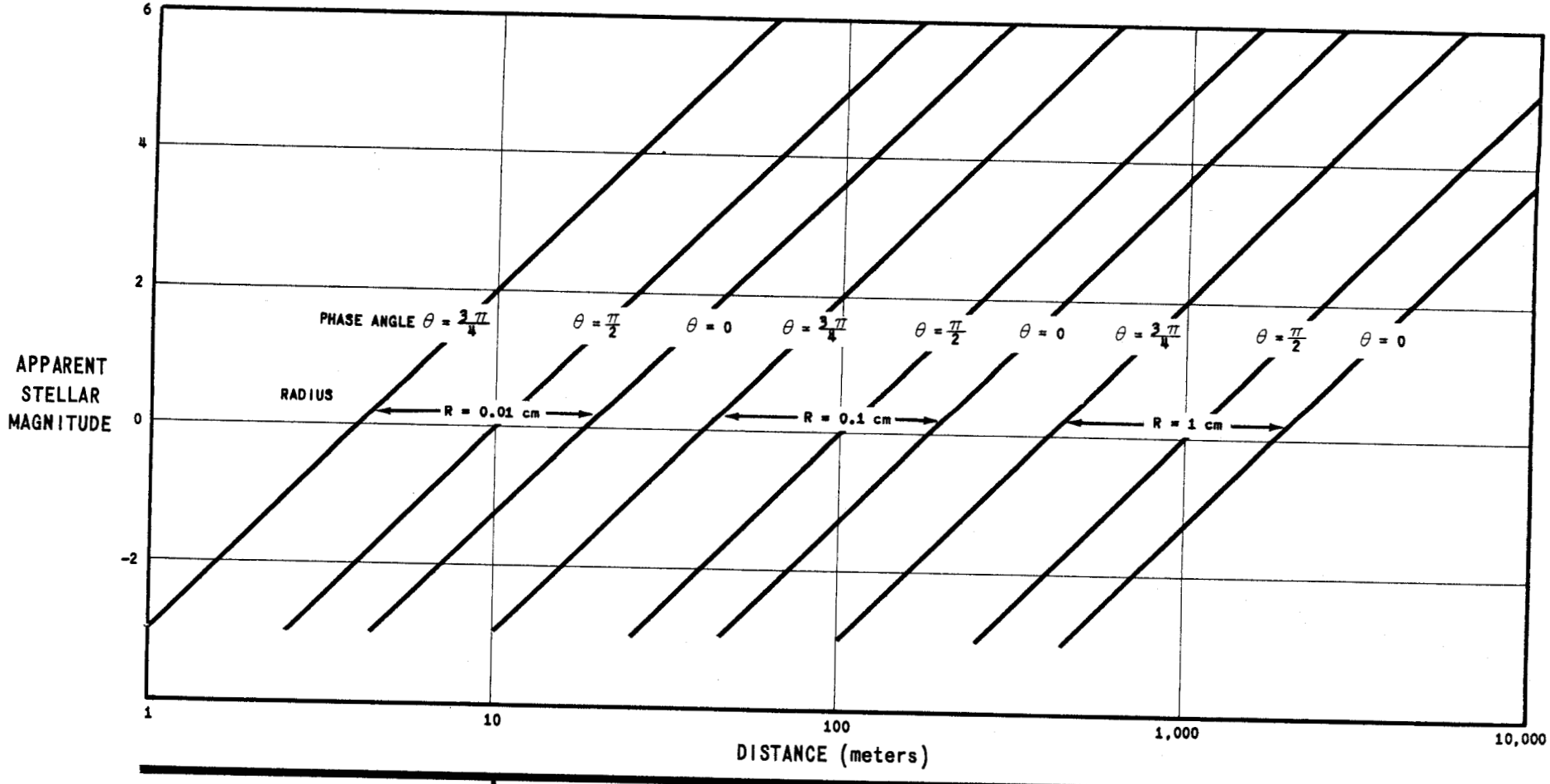

FIGURE 14

Apparent Stellar Magnitude of Meteoroids in Space as a Function of Distance From Observer

stellar magnitudes less than about 5 to 6. Thus, a 1 cm particle would be visible at distances of the order of tens of kilometers.

With Figure 14 as a basis, it is possible to estimate the maximum time available to carry out a protective maneuver against a particle on a collision course with the vehicle. Let us assume that a particle can be differentiated from the stellar background when its distance from the vehicle is such that the intensity of light reflected from it is some fraction "α" of the stellar background. Also, let us assume that the detector will have an aperture of Ψ radians, so that $2\pi/\Psi$ detectors are required to view the entire sky. Then the minimum intensity of light from the meteoroid which can be detected against the stellar background is

$$I_m = \alpha \Psi I_{st} \tag{53}$$

where I_{st} is the mean flux per steradian from the sky background. (It should be noted that such an instrument will not be able to look in the direction of any of the planets or their satellites when the vehicle is in their vicinity. Furthermore, it will not be able to look at the sun.)

For example, if we assume that Ψ is 0.01 of the total solid angle or 3.6%, and α is ten per cent, then using the value of 10^{-8} I_s for I_{st}, we calculate the minimum detectable flux to be 6×10^{-11} I_s watts/cm^2. This minimum flux corresponds to an apparent visual magnitude of -1. The corresponding distance from the vehicle at which the particle can be detected now can be read from Figure 14. This distance is plotted in Figure 15 as a function of particle radius for a number of different phase angles. Now if we assume that the instrumentation can determine the course of the meteoroid at the instant of first observation, it is possible to estimate the time available for a protective maneuver as a function of particle size. This is simply the distance divided by the meteoroid velocity. This calculated time is also included in Figure 15. The time scale was calculated using a value

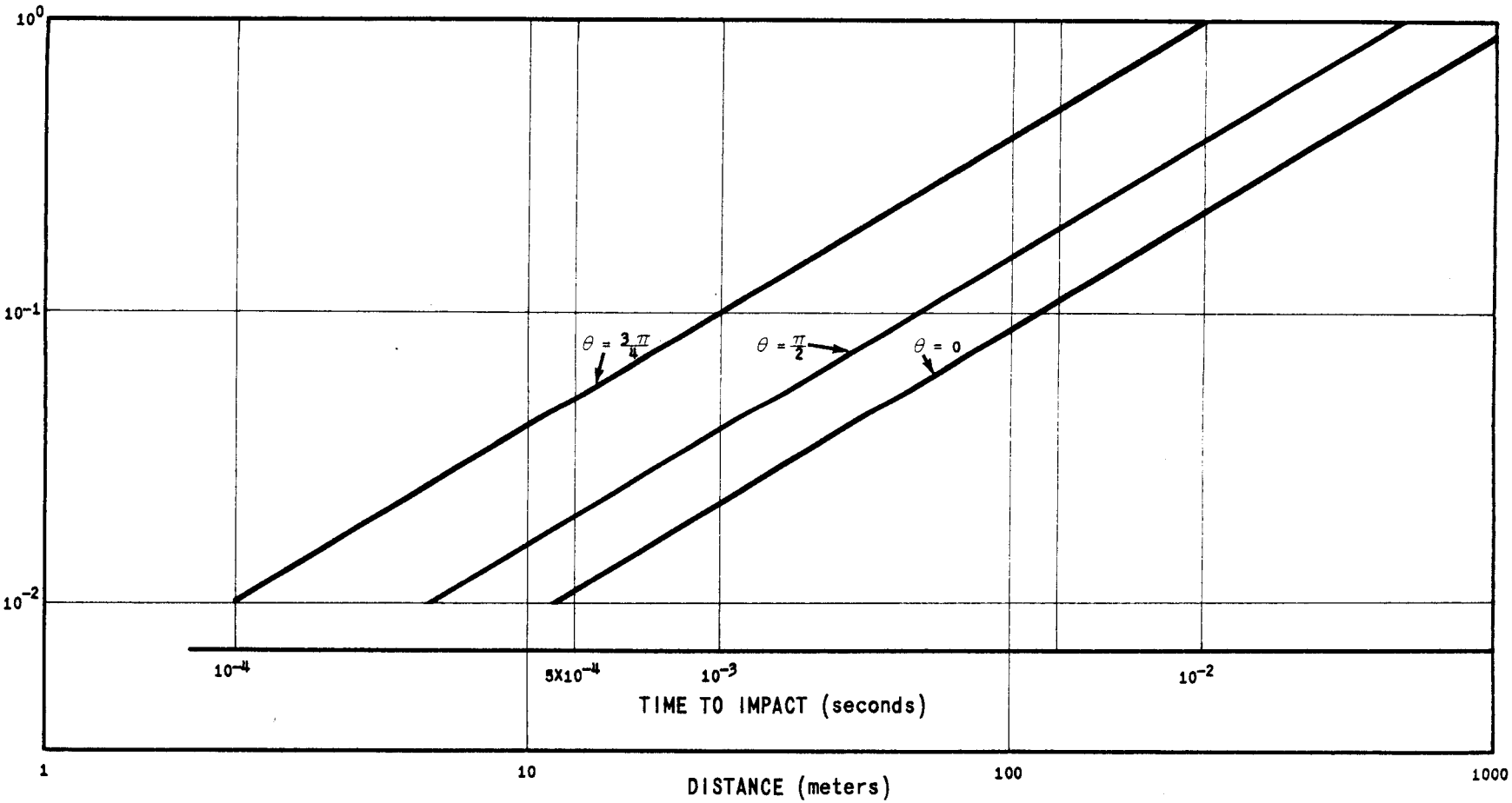

FIGURE 15

Distance at Which Various Size Meteoroids Can be Observed Against the Stellar Background and Time to Impact

of 25 KM/sec for the velocity. It may be noted that these time estimates are certainly optimistic, since the particle must be tracked to determine its course. Nevertheless, even in this overly optimistic procedure, the available times for particles in the size range of interest is from 10^{-4} to $4x10^{-2}$ seconds. If a ten-foot motion is required, this corresponds to accelerations in the range $4x10^{2}$ to $6x10^{7}$ g's. The engine thrust necessary to achieve such accelerations is 10^{4} to $2x10^{9}$ pounds per pound of material which is moved.

The implications of this short but conservative analysis are that an active meteoroid protection system is not feasible. The power requirement for accelerating even a small movable bumper is so large as to render such a scheme unreasonable. The only way to reduce this power requirement to a reasonable magnitude would be to increase the time available for maneuvering as the power needed is inversely proportional to the square of the duration of a maneuver. This implies detection of the particle at a farther distance. Reasonable power sources would require maneuver times of the order of seconds, which for a meteoroid moving at 25 kilometers per second, corresponds to an observation distance of about 100 kilometers. Currently, detection of particles in the size range of importance at such distances is not feasible by optical methods. Observation by other techniques, either active or passive, is highly unlikely.

IV. EFFECTS OF IONIZING RADIATION

A. THE CALCULATION OF RADIATION DOSE RATES

During this period, we have carried out a study to develop principles and methods for the calculation of radiation doses in space vehicles. Although this work was oriented toward evaluating the dosage which would be received by a liquid propellant in a tank, the treatment is generally applicable to any mass in a space vehicle. A technical report describing this work is now being prepared. (Report No. 63270-05-01 by R. D. Evans). The radiation considered in this effort consists of protons in the energy range from 10 Mev up to about 1000 Mev, and electrons in the energy range from 10 kev to about 1000 kev. The theory developed for protons is equally applicable to calculate dosage produced by any of the heavier particles in the cosmic radiation.

Because the spectrum and intensity of electrons and, more particularly, protons is known at present only approximately, and has been shown to vary enormously with time, a parametric treatment has been chosen. The radiation effects were calculated separately for each of several mono-energetic groups of protons and of electrons. The resulting values of this parametric treatment can be integrated for any energy spectrum. In addition, this procedure permits a clearer view of the physics of the phenomena and preserves a flexibility which is absent in the more conventional treatments where a particular assumed spectrum and intensity have been folded into the calculations as a first step, instead of a last step.

Our analysis has been very much concerned with the effects of angle of incidence of the radiation on penetration and dosage, since much of the radiation in space appears to be distributed in all directions. The study also considers the distribution of dose with depth into the propellant, rather than just the surface dose.

These results of this treatment differ markedly therefore from those which have been obtained previously from the "straight-through," surface-dose theory in which all radiations are assumed to strike a plane surface at normal incidence.

The analysis was divided into three portions, one on the effects of angularity of incident flux, one on proton doses, and one on the bremsstrahlung doses from incident electrons. It was shown in the first that Lambert's law applies to the calculations of the intensity of omnidirectional radiation flowing through a plane area per unit solid angle. In the second part, the dosage at the inside surface resulting from incident protons was calculated for liquid hydrogen, taking into account the effects of angularity on the penetration of protons through the walls of the container. A rough but useful approximation for the dosage at various depths and through various thicknesses of shields was also developed. A comparison was made between the approximate (straight-through) and exact theory for three different wall configurations: (1) 0.030-inch stainless steel; (2) 0.40 g/cm^2 of aluminum and glass wool + 0.030-inch stainless steel; and (3) 0.40 g/cm^2 aluminum and glass wool + 0.100-inch stainless steel.

As an order-of-magnitude illustration, these calculations were applied to the proton spectrum in the inner van Allen belt, as reported by Freden and White (20) in which the spectrum was represented as the power function,

$$\frac{1}{4}\,\Phi(E) = 1700\,E^{-1.8} \quad \frac{\text{protons}}{\text{sec.cm}^2\ \text{steradian Mev}} \qquad (54)$$

where $\Phi(E)$ is the omnidirectional flux of proton having energy between (E) and (E+dE)

The calculated total dose at the surface of liquid hydrogen shielded by 30 mil stainless steel (for an energy range extending from 40 Mev to about 1000 Mev) is about 1 rad/hr.

The expressions developed in the study demonstrate that for protons the dose is determined by the total flux of protons having energy greater than is required just to penetrate the container walls, and is nearly independent of the energy spectrum of these protons.

The estimation of radiation dose from absorbed bremsstrahlung was developed from empirical range-energy relationships for mono-energetic electrons and the theory for thick-target generation. The distribution of the primary bremsstrahlung was determined with calculations shown for three photon energies; 30, 80 and 500 kev. A calculation based on data of van Allen and Frank from Pioneer IV was made in which the primary dose received by the propellant near the tank wall, for a 30-mil thick stainless steel tank, was found to be

$$\sum R_{prim.} = 3.4 \frac{rad}{hr} \quad \text{in } H_2 \tag{55}$$

$$\sum R_{prim.} = 2.0 \frac{rad}{hr} \quad \text{in } O_2 \tag{56}$$

Estimates of the total dose (distinguished from the primary) are also included. It is shown that, at most, the secondary dose rate equals the primary dose rate, so that the total dose rate therefore can not exceed twice the primary dose rate.

B. EFFECT OF PROTON SPUTTERING ON ABSORPTIVITY AND EMISSIVITY OF REFLECTING SURFACES

As mentioned in our last report (21), protons from solar winds, solar flares or the inner van Allen belt may cause sputtering of surface layers of materials, with attendant changes in thermal absorptivity and emissivity. For example, thin layers of oxide on aluminum may be sputtered off to expose an oxide-free layer of aluminum metal. Figure 16 shows the change in total emissivity of a polished aluminum surface at 38°C as a function of thickness of an oxide layer deposited on the surface electrolytically. In this figure it may be noted that the

emissivity changes from 0.60 to 0.08 as the oxide thickness changes from 7×10^{-5} to 1.8×10^{-5} inches, i.e., 2800 to 700 angstroms. It is interesting to note that oxide layers of a few thousand angstroms can significantly affect emissivity.

Reiffel's estimate for thickness of oxide removed by proton sputtering gives values of 300 angstroms per month for solar winds during a "quiet period" and 300 angstroms per single encounter with an average solar flare (22).

A polished aluminum surface, displaying a typical value for emissivity of 0.12, might then have 3600 angstroms (10^{-4} inches) of oxide removed in a 12-month period due to solar winds during quiescent periods of the sun. (During active periods this may be twice as much.) From Figure 16, this could change the emissivity from 0.12 to about 0.04 for a thin oxide coating. In arriving at these conclusions, it was assumed that each incident particle sputters one atom. This is a liberal assumption and the yield for protons may be as much as one order of magnitude lower.

In reality, the sputtering yield depends upon numerous factors, the most important of which are the atomic number and the energy of the impinging ion and the chemical nature of the target material (23). Most observers agree that the sputtering yield increases with the atomic weight of the impinging ion at a rate considerably less than direct proportionality. Values greater than one have been achieved only with high atomic weight nuclei, and yield values higher than 10 have not been reported for any material. In view of this, it would be expected that hydrogen, which is the principal positive ion constituent of the solar winds and solar flares, should have a very low sputtering yield. In addition, it has been observed that at lower energy the yield depends markedly upon the energy of the impinging ion. Yields with hydrogen ions tend to level off at a value below 0.5 at an energy of 1 kev.

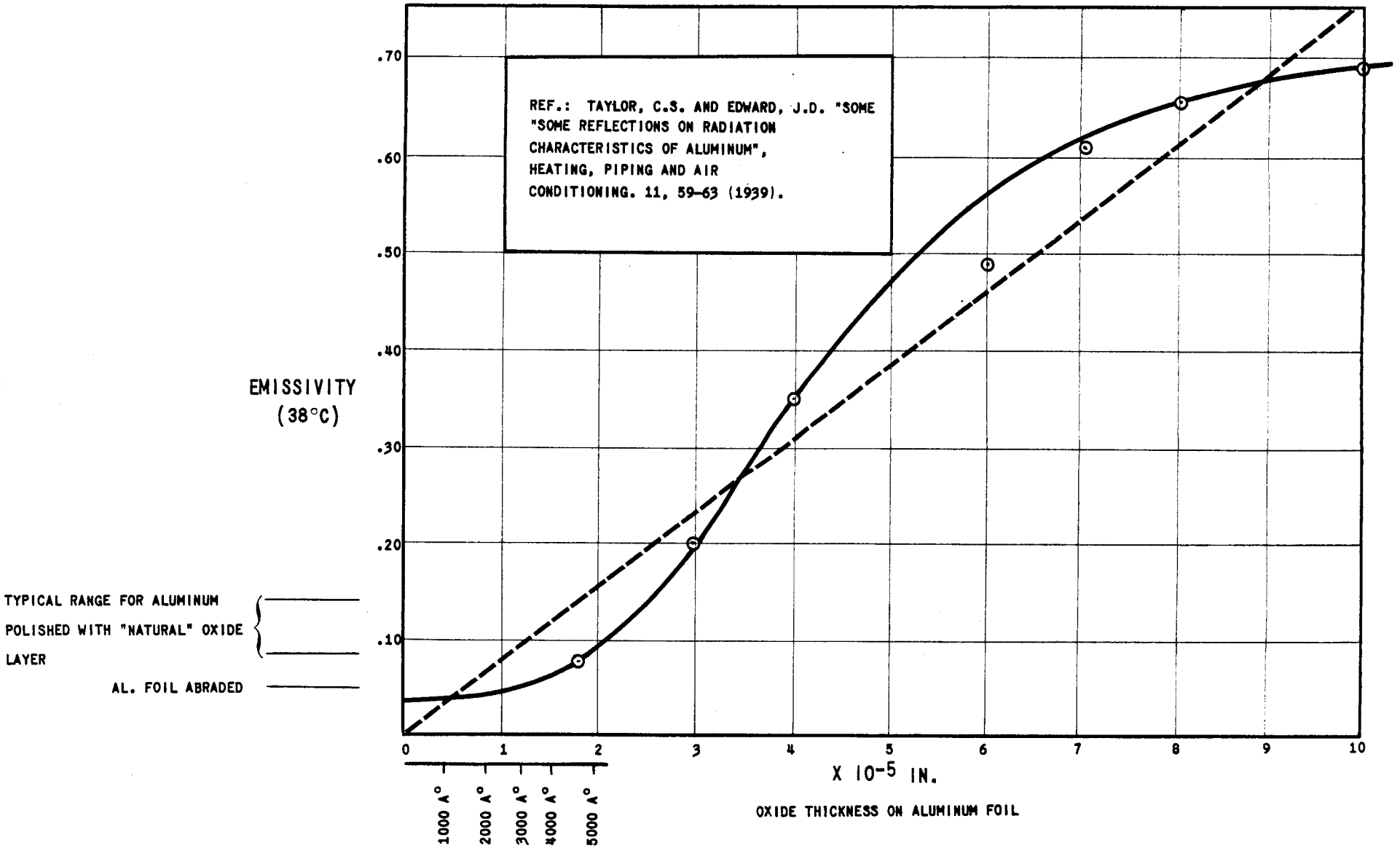

FIGURE 16 | Total Emissivity vs Oxide Thickness:Polished Aluminum

The nature of the substrate is also of prime importance with regard to the sputtering yield. For example, aluminum oxide has an unusually low sputtering yield presumably because of its high heat formation and sublimation. There appears to be a qualitative inverse relationship between the heat of sublimation of the target material and the sputtering yield. Materials of high sputtering rate include cadmium, copper and silver. Those with low sputtering rates include iron, tungsten, aluminum and magnesium. Sputtering yields of these metals with mercury, argon, neon and helium ion bombardment are in the range 0.4 to 2.5.

In view of the foregoing we are of the opinion that the assumption of a sputtering yield of unity although probably on the high side is reasonable for our considerations. Assuming this value and using existing data on proton flux and energy (21), we may discuss practical effects of proton sputtering on the storage of liquid propellants in space.

One of the problems associated with the storage of cryogenic liquids is the minimizing of the surface temperature. This requires minimizing the absorptivity-emissivity ration (α/ϵ) of the outer surface. The most promising materials for this purpose seem to be white oxides such as magnesium or aluminum oxide. Since proton sputtering might reduce the thickness of such layers at a rate of a few thousand angstroms a year, the outermost temperature control layer should be much thicker than this to prevent a change in emissivity. Based upon the sputtering rates estimated previously, this should be of the order of 10^{-4} to 10^{-3} inches. With such thicknesses, proton sputtering should not be a problem. If the estimates of the flux or sputtering yield which we have used prove to be much higher, the required oxide thicknesses would be raised accordingly.

The largest flux of protons impinging on the space craft appears to be associated with the solar winds. Energies of these protons are in the kilovolt range. Penetrability of kilovolt energy protons is so low that one need not be concerned with proton sputtering

inside the outer skin of the vehicle. Higher energy protons in the Mev range will be encountered during solar flares and while traversing the inner van Allen belt. The total number which would penetrate the outer skin and impinge on the inner shield surfaces of multi-foil radiation shielding is down many orders of magnitude from the number incident to the outer skin. Thus the sputtering rate on an inner shield can be considered negligible. Actually, sputtering of the inner reflective surfaces (such as aluminum) should be beneficial rather than detrimental since a reduction of emissivity is desirable.

One may conclude therefore that proton sputtering need not create problems due to changing absorptivity or emissivity characteristics of temperature controlling surfaces for liquid propellant vessels, unless present estimates of proton fluxes, energies, and sputtering yields prove erroneous. The outermost surface layer should have a sufficient thickness (probably greater than 10^{-4} or 10^{-3} inches) in order to survive proton sputtering.

We will continue to examine new data on proton flux and energies in space and to follow work being initiated elsewhere on proton sputtering yields. We will also follow the trend of approaches to the thermal insulation problem so that if any of the above assumptions (regarding thermal shield design) change or if the need for further data becomes evident, we can modify our present conclusions and make appropriate recommendations.

C. EMBRITTLEMENT OF STRUCTURAL MATERIALS

Structural requirements for cryogenic containers for liquid hydrogen require the materials of construction to have suitable mechanical ductility as well as strength at 20°K. It is well known that some metals are not useful because they become quite brittle at low temperatures and for this reason the following paragraphs are limited to a discussion of three principal ductile materials of construction -- stainless steel, aluminum alloys, and titanium alloys -- in terms of the possibility of embrittlement at this temperature.

1. Transformation Embrittlement at Low Temperatures

Austenitic stainless steel retains its ductility at low temperatures. The austenitic face-centered lattice is not the equilibrium structure for these alloys and is metastable even at ordinary temperatures. Some compositions, such as the well-known 18% chromium -- 8% nickel alloy, can partially transform to martensite, a hard and brittle structure, through deformation at room temperature. This transformation occurs to a greater extent at low temperatures and for this reason the 18-8 composition could, under the combined conditions of low temperature and stress, become embrittled by martensite formation.

This deleterious transformation may be almost entirely prevented by the use of an austenitic stainless steel which contains in excess of 20% nickel (24).

Neither aluminum nor alpha-strengthened titanium alloys are known to undergo embrittling transformation reactions such as those described above. Low-temperature mechanical tests have been made on both of these materials and there is every evident that, although they both undergo some embrittlement, these alloys retain adequate ductility at 20°K (25,26).

2. Hydrogen Embrittlement

Hydrogen embrittlement is known to impair the ductility of many metals, particularly at low temperature. Titanium and its alloys are notable in this respect. As little as ten parts per million of hydrogen significantly reduces the ductility of this metal. It should be emphasized that reaction rates for solution of hydrogen in titanium at low temperature are low and for this reason it should not be immediately presumed that titanium and its alloys are not suitable for containment of hydrogen at low temperatures.

In fact, excellent low temperature properties have been noted for a 5% Al--2.5% Sn alpha-strengthened alloy at liquid helium temperature, and a number of titanium alloys such as the 6% Al-4%V composition are now being used as cryogenic containers for liquid nitrogen. The

high strength weight ratios of titanium alloys require serious consideration of these materials for any space application.

There is no evidence of embrittlement of aluminum by hydrogen. Austenitic stainless steel is also considered to be highly resistant to hydrogen embrittlement.

3. Radiation Embrittlement

Metals, such as those used for the containment of cryogenic liquids, are embrittled by bombardment with high-energy particles. Radiation embrittlement by neutrons and ionized particles at ordinary temperatures is usually insignificant for integrated fluxes below 10^{19} particles per square centimeter. For space missions which do not involve the use of a nuclear reactor, the only significant radiation will be in the form of high-energy protons. This flux is expected to be less than 10^{4} particles/cm^{2} sec and the integrated dose for a one-year period (3.2×10^{7} seconds) should not cause significant radiation damage. One important point in this connection is the observation that the resistance of metals to radiation damage is largely a result of annealing-out of radiation damage at ordinary temperatures. At low temperatures this process is significantly reduced and the cumulative radiation damage which would result from an extended mission which involves the use of a nuclear reactor might be significant.

D. EFFECT OF HYDROGEN DIFFUSION ON VACUUM INSULATION

As noted previously, (see also Section II,B of this report) multi-foil insulation surrounding a cryogenic shell requires the maintenance of a pressure below approximately 10^{-5} to 10^{-4} mm of mercury for effective performance. If the shield insulation is not vented to space, gas pressure may build up in it, causing ineffective performance. To estimate the possibility of this occurrence various mechanisms for buildup should be considered and evaluated. The following discussion considers, first, the possibility of hydrogen diffusion through the tank shell, and second, the buildup of hydrogen from high-energy protons which are stopped in the insulation.

1. Diffusion in the Absence of Radiation

The rate of transport of hydrogen through the wall of a metal barrier can be represented by the following statement:

$$J = D_o e^{-\frac{Q}{RT}} \frac{\partial C}{\partial x} \qquad (57)$$

where J = The number of mols of hydrogen diffusing through one square centimeter of the wall per second

$\frac{\partial C}{\partial x}$ = concentration gradient in the wall expressed as mols/cm^3/cm or $\frac{ccSTP}{cm^3\text{-}cm}$

D_o = diffusion constant at very high temperature (cm^2/sec) ($D_o e^{-Q/RT}$ is the diffusion constant at temperature T)

Q = activation energy for diffusion (cal./mol)

T = temperature (°K)

R = gas constant

To a first approximation:

$$\frac{\partial C}{\partial x} = \frac{C_1}{L} \qquad (58)$$

where C_1 = concentration of hydrogen in the wall on the high-pressure side

and L = wall thickness.

Hydrogen normally dissolves into the interstices of a metal lattice as the atomic specie. Consequently, the first step in solution, and thence diffusion, must be dissociation of the molecular hydrogen; i.e. $H_2 \longrightarrow 2H$, at the surface of the metal. The equilibrium constant for this process may be written as

$$K_D = (H)^2/P_{H_2} \qquad (59)$$

where P_{H_2} is the pressure of molecular hydrogen in contact with the surface.

(H) is the concentration of atomic hydrogen

and K_D is the equilibrium constant for dissociation.

The concentration of atomic hydrogen in the metal, C_1, is proportional to its concentration at the surface, (H). This statement coupled with equation (59) implies that

$$C_1 = k_2 P_{H_2}^{1/2} \tag{60}$$

Equation (60) above is a statement of Sievert's law. Substitution of equations (58) and (60) in equation (57) gives a more useful form of the diffusion equation, namely,

$$J = \frac{D_o e^{-\frac{Q}{RT}} k_2 P_{H_2}^{1/2}}{L} \tag{61}$$

We are now in a position to obtain an estimate of the quantity of hydrogen which can diffuse through the container wall into the multi-foil shielding. For liquid hydrogen at one atmosphere pressure, T = 20°K. D_o is typically of the order of 10^{-2} $cm^2/sec.$, and Q for most metals is approximately 10,000 calories per mol. If we use a low value for Q, 3,400 calories per mol, the estimate in the calculated diffusion rate will err on the high side. Using these values, for a 30-mil thick tank (0.075 cm); $J = 10^{-38} k_2$ $mols/cm^2/sec.$ At room temperature k_2 is of the order of 10^{-6} to 10^{-3} $mols/cm^3\text{-}atm^{1/2}$. Although there is no data for the container materials of interest at the temperature of liquid hydrogen, it can be expected that k_2 will be appreciably lower than the room temperature value. Thus J will be less than 10^{-41} $mols/cm^2/sec.$ This rate of leakage into shields separated by $5x10^{-3}$ cm. will produce pressure buildup at 20°K at a rate of $2.5x10^{-33}$ mm of mercury per second or a total buildup of $8.0x10^{-26}$ mm per year. This is a negligible rate under any circumstances, especially since these estimates are on the high side.

Another calculation can be made with the use of permeation data, which takes surface reactions into consideration (27). Extrapolating empirical data to 20°K gives rates of pressure increase under the same conditions as above of 10^{-320} mm/year. It is clear that diffusion, in the absence of radiation, is not a problem.

2. The Effect of Radiation on Hydrogen Diffusion

Ionizing radiation may be expected to increase the diffusion rate of hydrogen through a metal barrier by creating mobile hydrogen species, the atomic (H•) and ionic or proton (H^+), over and above the amount normally present. These additional species increase the concentration, which is the driving force for diffusion across a barrier. The rate at which these species are produced by radiation can be expressed by the following equation

$$I = 1.23 \times 10^{12} \rho \, G \, d_R \qquad (62)$$

where

I = rate of production in atoms/cc-sec.

ρ = substrate density in gm/cc.

G = quantum effectiveness in molecules reacted/100EV absorbed

d_R = dose rate in rads/sec.

The species produced have a tendency to recombine and return to the molecular form through a reaction scheme which includes the following steps:

$$H^+ + e^- \longrightarrow H\bullet \qquad (A)$$

$$2H\bullet \longrightarrow H_2 \qquad (B)$$

The precise kinetics for this scheme of reactions are not readily defined. However, because of the electrostatic fields associated with the species H^+ and the electron, and the absence of an equivalent potential field about the atomic species (H•), it is reasonable to assume

that reaction A will occur at a much greater rate than reaction B. Thus, the limiting process in the recombination to form molecular hydrogen should be reaction B. Thus for kinetic analysis it may be assumed that the net effect of the ionizing radiation is to produce hydrogen atoms.

In order to determine in a rigorous manner the number of atoms permeating the wall, it would be necessary to obtain a solution to the diffusion equation, including terms for the reactions. This procedure is complicated and difficult to generalize. There is, however, an approximate treatment available, based on kinetic theory, which enables us to calculate the maximum possible flux across a barrier.

The concentration of atomic hydrogen dissolved in the liquid molecular hydrogen will be shown to be very low. Because of this many aspects of the behavior of the system are governed by the kinetic theory for gases. The mean free path between collisions of the atomic specie and the collision frequency can be calculated as if the solvent (molecular hydrogen) were not present (29). Each collision between two atoms should be effective in producing molecular hydrogen because the activation energy for free radical reactions is very low and because it is highly probable that a collision with a solvent molecule will occur nearly simultaneously, providing the third body necessary to stabilize the reaction product. With these statements as basic assumptions, we can proceed to calculate the flux of atomic hydrogen impinging on the wall. If we assume that all the atomic hydrogen hitting the wall will permeate, and that hydrogen diffuses only as the atomic species, then this calculation will yield a maximum estimate.

If, as above, we assume that every collision between two hydrogen atoms leads to a recombination to form molecular hydrogen (reaction B), then we can state that only those atoms, produced within the region bounded by the wall and extending into the liquid a distance

equal to the mean displacement between collisions, will reach the wall without undergoing a reaction. On the average all atoms which are farther away will undergo at least one collision, and reaction, before they could impinge on the wall. As a mathematical argument, this statement is equivalent to the expression

$$F = \frac{I\bar{x}}{6} \tag{63}$$

where

F = flux impinging on wall in $\frac{\text{atoms}}{\text{cm}^2\text{-sec}}$

I = rate of production of hydrogen atoms in $\frac{\text{atoms}}{\text{cc-sec.}}$

$\bar{x}$ = mean displacement between collisions in cm

The factor, one-sixth, arises because of the random distribution of motion. Only those atoms moving in the direction of the wall can hit the wall. On the average, this is one-sixth of the total number of hydrogen atoms in the region of interest. The other will move in such a direction that they will undergo a reactive collision prior to hitting the wall.

We must carefully examine the significance of the mean displacement between collisions ($\bar{x}$ in equation 63) for this system. As stated above, the magnitude of the mean free path for a solute in very dilute solution is identical to the magnitude of the path calculated as if the solvent was not present. The path traveled by a solute atom (H•) is, however, not a straight line, but follows the pattern of a random walk due to collisions with solvent molecules along the way. Thus, while the ordinary equation for mean free path determines the distance traveled between collisions, the displacement between the positions of successive collisions is determined by the diffusion relation (30).

$$\bar{x} = (2Dt)^{1/2} \tag{64}$$

where

D = diffusivity in $\frac{cm^2}{sec}$

t = time between collisions in $\frac{sec}{collision}$

The diffusivity is given as (30)

$$D = \frac{RT}{6\pi\eta r N} \tag{65}$$

where

R = gas constant in $\frac{ergs}{mol\text{-}^\circ K}$

T = temperature in °K

η = viscosity of solvent in poises (gm/cm-sec)

r = diameter of diffusion specie in cm

and N = Avogadro's number in atoms/mol

The time between collisions is equal to the mean free path divided by the mean speed.

$$t = \frac{\bar{l}}{\bar{v}} \tag{66}$$

where

$\bar{l}$ = mean free path in cm

$\bar{v}$ = mean speed in cm/sec

The usual kinetic theory formula for mean free path is (31)

$$\bar{l} = \frac{1}{\sqrt{2}\,\pi\, c\, \sigma^2} \tag{67}$$

where

c = concentration of atomic hydrogen in $\frac{atoms}{cc}$

σ^2 = effective collision area in cm^2/atom

The mean speed is given as (31)

$$\bar{v} = \left(\frac{8RT}{\pi M}\right)^{1/2} \tag{68}$$

where

M = molecular weight in gms/mol.

We assume that the atoms produced by the primary interaction with radiation would be thermalized in the first few collisions with the solvent (H_2), so that the ordinary kinetic theory expression for mean speed is valid.

Finally, before we can calculate the flux, F, we need to determine a proper value for concentration to use in equation 67 for the mean free path. If we assume that the rate of permeation through the walls is small compared to the rate of production, then the concentration will reach a steady state value so that the rate of production just equals the rate of recombination. Continuing our kinetic theory argument, this statement is equivalent to

$$c_{ss} = (I/k)^{1/2} \tag{69}$$

where k = collision frequency

The collision frequency, k, for bimolecular collisions between like molecules, is

$$k = 2\sigma^2 \left(\frac{\pi RT}{M}\right)^{1/2} \tag{70}$$

Equations 63 to 70 can be combined to obtain an expression for the flux F.

$$F = \frac{I^{3/4}}{6(\pi r \eta N \sigma)^{1/2}} \left[\frac{M(RT)^3}{5184\pi}\right]^{1/8} \tag{71}$$

For reactions occurring in liquid hydrogen at 20°K, where

$$r = \sigma \cong 10^{-8} \text{ cm}$$

$$\eta = 1.4 \times 10^{-4} \text{ poise},$$

the equation after evaluating the constants is

$$F = 0.88\ I^{3/4} \tag{72}$$

We are now in a position to calculate the flux of hydrogen atoms to a wall in space. The rate of production of hydrogen atoms, I, can be obtained from equation (62), given the dose rate (d_R) and the G value for the dissociation. Based on the work of R. D. Evans (Section IVA), the maximum average radiation dose rate can be expected to be about 10 rads per hour or 0.0028 rad per second. The G value for the formation of ionization products is estimated to be 10. This represents a yield of 20 hydrogen atoms for every 100 e. v. absorbed, a value which is roughly half the theoretical maximum based on bond energies. Based on these numbers

$$I = 2.4 \times 10^{9} \text{ atoms/cc-sec}$$

and

$$F = 9 \times 10^{6} \ \frac{\text{atoms}}{\text{cm}^2\text{-sec}}$$

This estimation of flux should be the maximum possible with the given dose. We would expect the actual magnitude to be less for several reasons. First, a surface is usually a promoter for recombination reactions, so that some of the atoms reaching the wall would recombine on the surface and be unable to permeate. The catalytic activity of a surface is very sensitive to its history; there are some scattered data available to indicate this. Data taken for the permeation of aluminum alloys by hydrogen at 500°C show that the permeability can vary over several orders of magnitude, depending on surface treatment, and over a larger range in the presence of a glow discharge (28). Thus, it may be possible that actual permeation rates are down from our maximum estimate by several orders of magnitude.

Secondly, our treatment implicitly assumes that active species are produced uniformly throughout the vessel. In fact, in radiation induced reactions the primary reaction products are formed in the vicinity of the radiation track. In this case, we would expect recombination to occur more rapidly than would be the case if the reaction proceeded uniformly throughout the entire volume, since the

concentration of active species in the reaction zone is high. This is effectively an entrapment of the active species, reducing the number available for diffusion to the wall.

To determine whether a flux of the magnitude predicted above could cause a serious problem, we refer to the results of our study on the effects of gases on insulation behavior. Table II of this report is a summary of the effect of outgassing on thermal conductivity. Hydrogen permeation acts in the same way as outgassing. For a vented multilayer insulation system, the problem of outgassing is not serious until the rate reaches about 10^{12} molecules/cm^2-sec. The maximum estimate above of about 10^7 molecules/cm^2-sec is so far down in magnitude that we anticipate that no problems due to hydrogen diffusion into the insulation should arise in a vented system.

On the other hand, if the insulation is sealed, a pressure rise due to the containment of hydrogen diffusing out may become serious in long voyages.

From the perfect gas law, the pressure rise in an annular region of spacing, s, is equal to

$$P = \frac{FR\bar{T}}{2Ns}\ominus \tag{73}$$

where

$\ominus$ = time in seconds
s = spacing in centimeters
F = flux in atoms/cm^2-sec
$\bar{T}$ = average temperature in annulus in °K

Using the value of F calculated above and a value of 140°K for $\bar{T}$, this becomes

$$P = 7 \times 10^{-11}\ \frac{\ominus}{s} \tag{74}$$

If we assume that the entire void volume of the insulation is filled with gas, then in one year the pressure rise in one inch of insulation would be about 2×10^{-3} mm. This pressure rise would seriously

affect the capacity of the insulation. Because of the uncertainty in permeation rates caused by recombination at the surface as described above, this estimate may be several orders of magnitude high. We believe that the problems would be marginal or non-existent in real systems because of this. However, we also believe that if a sealed system were to be seriously considered for use, it would then be advisable to determine experimentally the permeability of metals under a variety of conditions to substantiate the conclusions of this theoretical argument.

With the above statements as a summary for sealed systems, we conclude with a summary statement for vented system. Hydrogen diffusion in the presence of radiation through the walls of a tank will not affect the operation of multilayer radiation shielding if the insulation is vented or pumped. This treatment can be applied to the effects arising from the radiation field of a nuclear reactor, by using the proper value for yield, G, for neutron interactions in the calculation for the rate of formation, I. The remainder of the analysis is unchanged.

3. Hydrogen Production by Proton Capture

Hydrogen may be formed within multiple-foil insulation, through the mechanism of proton capture. Protons incident to a storage tank may extract electrons as they pass through the metal layers of the insulation and be transformed into atomic hydrogen. If the atomic hydrogen can diffuse out of the laminae into the interstices, gas buildup will occur.

Using a value for proton flux of 10^4 protons/cm^2-sec., which value is typical of the proton flux in the inner van Allen belt, we calculate that the pressure rise in a one-centimeter layer of insulation would be about 5×10^{-6} mm per year. This rate is small but could be significant for extended missions, if the insulation was sealed within protective walls.

E. RADIATION-INDUCED DESORPTION OF ADSORBED GASES

In our previous report (21) we made a preliminary estimate of the effect of the energetic protons in solar flares and in the inner van Allen belt on adsorbed molecules in multilayer insulation. We now believe that the assumption that 10 adsorbed molecules of gas would be displaced by one proton from each surface should be revised downward to a value of 1 molecule per proton. The effects of displacing physically adsorbed molecules were found to be insignificant with the high estimate and remain insignificant.

The effects of removing chemically adsorbed gases even with the lower value for yield for proton, may be significant in a sealed insulation system on extended trips. The difference between the effects in these two cases arises because chemisorbed molecules are not easily reabsorbed at low temperatures. There is generally a considerable energy barrier for reabsorption (30-60 kcal/mole) which cannot be broached by the desorbed species.

V. REFERENCES

1. Burry, R. V. and V. R. Degner, Liquid Propellant Storage Evaluation for Space Vehicles, 4th Symposium on Ballistic Missiles and Space Velocity, U.C.L.A., August 1959.

2. Smolak, G. R. and R. H. Knoll, Cryogenic Propellant Storage for Round Trips to Mars and Venus, I.A.S. 28th Meeting, New York, January 1960.

3. Smolak, G. R. et al., Analysis of Thermal Protection System for Space Vehicle Cryogenic Propellant Systems, Review Copy, NASA Report to be published.

4. Black, I. A. et al., Advances in Cryogenic Engineering, Volume 5, Plenum Press, New York, 1960, p. 181.

5. Kropschot, R. H. et al., Ibid. p. 189.

6. Hnilicka, M. P., Ibid. p. 199.

7. Riede, P. M. and D. I.-J. Wang, Ibid. p. 209.

8. Abarbanel, S. S., On Some Problems in Radiative Heat Transfer, M.I.T. Report 59-1, April 1959.

9. Whipple, F. L., "Possible Hazards to a Satellite Vehicle", Project Rand Douglas Aircraft Corporation, Santa Monica, California, 1946 (SECRET).

10. Willig and Semon, "A Multi-stage H.E. Actuated Hypervelocity Gun", Proceedings of the Third Symposium on Hypervelocity Impact, Armour Research Foundation, pp. 507-509, February 1959.

11. Olshaker, A. E., "An Experimental Investigation in Lead of the Whipple Meteor Bumper", Thesis for M.S. Degree M.I.T., 1960.

12. Hopkins, H. G. and H. Kolsky, Mechanics of Hypervelocity Impact of Solids, A.R.D.E. Report (B) December 1960, Fort Halstead, Kent.

13. Maiden, C. J., J. Charist and H. P. Tardif, An Investigation of Spalling and Crater Formation by Hypervelocity Projects, Proceedings of Fourth Symposium on Hypervelocity Impact, Volume 3, 1960.

14. Proceedings of Third and Fourth Symposia on Hypervelocity Impact, 1959, 1960.

15. Stanyukovich, K. P. Unsteady Motion of Continuous Media, Pergamon Press.

16. Courant and Friedrichs, Supersonic Flow and Shock Waves, Academic Press.

17. Pack, D. C., W. M. Evans and H. J. James, The Propagation of Shock Waves on Steel and Lead, Proceedings of the Physical Society, Volume 60, Part 1, January 1948, No. 337.

18. Shternfield, A., Iskusstvennye Sputniki, Gostekhizdat, Moscow 1958.

19. Levin, B., "Artificial Earth Satellites and Meteors", Meteoritika, 18 (1960).

20. Freden, S. C. and R. S. White, Phys. Rev. Letters 3, 9 (1959); J. Geophysical Res. 65, 1377 (1960).

21. "Liquid Propellant Losses During Space Flight", NAS 5-664, January 1961, p. 51.

22. Reiffel, L., "Structural Damage and Other Effects of Solar Plasmas", ARS Journal, March 1960, p. 260.

23. Wehner, G. K., "Sputtering by Ion Bombardment", Advances in Electronics and Electron Physics, Volume 7, 1955, pp. 239-297, Academic Press.

24. Ziegler, N. H., Hardening of Austenitic Stainless Steels by Mechanical Working at Sub-zero Temperatures, p. 878 (Ref. 772).

25. Cryogenic Materials Data Handbook, National Bureau of Standards, U. S. Department of Commerce (1959).

26. Timmerhaus, K. D. Ed., Advances in Cryogenic Engineering, Volume 1, Plenum Press (1960) p. 238.

27. Smithelis, C. J., Gases and Metals, London (1937).

28. Cochran, C. N., "The Permeability of Aluminum to Hydrogen", Journal of Electrochemical Society, 108, pp. 317-321 (April 1961).

29. Hinshelwood, C. N., The Structure of Physical Chemistry, Oxford University Press, London 1951.

30. Glasstone, S., Textbook of Physical Chemistry, D. Van Nostrand Company, Inc., New York 1946.

31. Kennard, E. H., Kinetic Theory of Gases, McGraw-Hill Book Company, Inc., New York 1938.